






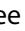






BASIC RESEARCH PAPER

## Autophagy induced by AXL receptor tyrosine kinase alleviates acute liver injury via inhibition of NLRP3 inflammasome activation in mice

Jihye Han <sup>a,†</sup>, Joonbeom Bae <sup>a,†</sup>, Chang-Yong Choi <sup>a</sup>, Sang-Pil Choi <sup>a</sup>, Hyung-Sik Kang <sup>b</sup>, Eun-Kyeong Jo <sup>c</sup>, Jongsun Park <sup>d</sup>, Young Sik Lee <sup>a</sup>, Hyun-Seuk Moon <sup>a</sup>, Chung-Gyu Park <sup>e</sup>, Myung-Shik Lee <sup>f</sup>, and Taehoon Chun <sup>a</sup>

<sup>a</sup>Department of Biotechnology, College of Life Sciences and Biotechnology, Korea University, Seoul, Korea; <sup>b</sup>School of Biological Sciences and Technology, Biotechnology Research Institute, Chonnam National University, Kwangju, Korea; <sup>c</sup>Infection Signaling Network Research Center, Department of Microbiology, College of Medicine, Chungnam National University, Daejeon, Korea; <sup>d</sup>Department of Pharmacology, Metabolic Diseases and Cell Signaling Laboratory, Research Institute for Medical Sciences, College of Medicine, Chungnam National University, Daejeon, Korea; <sup>e</sup>Department of Microbiology and Immunology, Seoul National University College of Medicine, Seoul, Korea; <sup>f</sup>Severance Biomedical Science Institute, Department of Internal Medicine, College of Medicine, Yonsei University, Seoul, Korea

### ABSTRACT

Severe hepatic inflammation is a common cause of acute or chronic liver disease. Macrophages are one of the key mediators which regulate the progress of hepatic inflammation. Increasing evidence shows that the TAM (TYRO3, AXL and MERTK) family of RTKs (receptor tyrosine kinases), which is expressed in macrophages, alleviates inflammatory responses through a negative feedback loop. However, the functional contribution of each TAM family member to the progression of hepatic inflammation remains elusive. In this study, we explore the role of individual TAM family proteins during autophagy induction and evaluate their contribution to hepatic inflammation. Among the TAM family of RTKs, AXL (AXL receptor tyrosine kinase) only induces autophagy in macrophages after interaction with its ligand, GAS6 (growth arrest specific 6). Based on our results, autophosphorylation of 2 tyrosine residues (Tyr815 and Tyr860) in the cytoplasmic domain of AXL in mice is required for autophagy induction and AXL-mediated autophagy induction is dependent on MAPK (mitogen-activated protein kinase)14 activity. Furthermore, induction of AXL-mediated autophagy prevents CASP1 (caspase 1)-dependent IL1 $\beta$  (interleukin 1,  $\beta$ ) and IL18 (interleukin 18) maturation by inhibiting NLRP3 (NLR family, pyrin domain containing 3) inflammasome activation. In agreement with these observations, *axl*<sup>-/-</sup> mice show more severe symptoms than do wild-type (*Axl*<sup>+/+</sup>) mice following acute hepatic injury induced by administration of lipopolysaccharide (LPS) or carbon tetrachloride (CCl<sub>4</sub>). Hence, GAS6-AXL signaling-mediated autophagy induction in murine macrophages ameliorates hepatic inflammatory responses by inhibiting NLRP3 inflammasome activation.

### ARTICLE HISTORY

Received 23 December 2015  
Revised 24 August 2016  
Accepted 7 September 2016

### KEYWORDS

autophagy; AXL receptor tyrosine kinase; hepatic inflammation; macrophage; NLRP3 inflammasome



## Introduction

Liver disease is often initiated by severe hepatic inflammation which mediates progressive liver damage and fibrosis.<sup>1,2</sup> During hepatic inflammation, macrophages act as sentinels which initiate immune responses and provide important mediators for wound healing and metabolic functions.<sup>3,4</sup> Therefore, regulating the activity of macrophages provides an excellent therapeutic strategy to alleviate severe hepatic inflammation.

The TAM family of RTKs expressed in macrophages negatively regulates inflammatory responses by not only facilitating the clearance of apoptotic bodies,<sup>5,6</sup> but also by providing signals which inhibit inflammation.<sup>7,8</sup> Indeed, TAM-deficient (*tyro3*<sup>-/-</sup>, *axl*<sup>-/-</sup>, *merlk*<sup>-/-</sup>) mice or *Mertk* mutant mice develop spontaneous lymphoproliferative diseases such as the autoimmune disease lupus.<sup>9,10</sup>


Previous observations show that the interaction between the TAM family of RTKs and their common ligand, GAS6, plays a protective role during liver inflammation. In a murine ischemia and reperfusion injury model, *Gas6*-deficient (*gas6*<sup>-/-</sup>) mice show more severe hepatic injury than do wild-type (*Gas6*<sup>+/+</sup>) mice, and treatment of *gas6*<sup>-/-</sup> mice with exogenous GAS6 rescues the phenotype.<sup>11</sup> In a murine model of CCl<sub>4</sub>-induced liver injury, *Gas6* deficiency delays wound healing.<sup>12</sup> Since GAS6 is a common ligand of all TAM RTKs, the specific role of each TAM family member in the progress of hepatic inflammation remains to be determined.

Autophagy is a homeostatic degradative process that removes damaged organelles or turns over cytoplasmic constituents via lysosomal compartments in eukaryotic cells.<sup>13</sup> Although autophagy was initially identified to enhance cell

**CONTACT** Taehoon Chun  [tchun@korea.ac.kr](mailto:tchun@korea.ac.kr)  Department of Biotechnology, College of Life Sciences and Biotechnology, Korea University, Seoul, 02841, Republic of Korea.

Color versions of one or more of the figures in the article can be found online at [www.tandfonline.com/kaup](http://www.tandfonline.com/kaup).

<sup>†</sup>These authors contributed equally to this work.

 Supplemental data for this article can be accessed on the publisher's website.

© 2016 Taylor & Francis

survival, increasing evidence shows that autophagy is involved in a variety of biological events.<sup>14,15</sup> In particular, recent observations have demonstrated an inverse relationship between autophagy induction and maturation of NLRP3 inflammasomes in macrophages.<sup>16–18</sup> Therefore, autophagy may regulate proinflammatory cytokine production via inhibiting activation of the NLRP3 inflammasome in macrophages, which in turn may contribute to the symptoms of specific inflammatory diseases.<sup>19,20</sup>

Given the above information, we explored the role of individual TAM family members during autophagy induction and evaluated their roles in hepatic inflammation. We found that the interaction between AXL and GAS6 induced autophagy via autophosphorylation of 2 tyrosine residues within the cytoplasmic domain of AXL in a manner dependent on MAPK14. Furthermore, GAS6-AXL-mediated autophagy induction inhibited NLRP3 inflammasome activation, which led to reduced production of IL1 $\beta$  and IL18. In accordance with these observations, *axl*<sup>−/−</sup> mice showed more severe symptoms than did wild-type (*Axl*<sup>+/+</sup>) mice in acute hepatic injury models. Therefore, GAS6-AXL signaling inhibits inflammatory responses by inducing autophagy.

## Results

### Interaction between GAS6 and AXL induces autophagy in macrophages by increasing mRNA transcript levels of *Becn1*, *Atg5*, and *Map1lc3b*

To determine the effect of TAM receptor signaling on autophagy induction, we first analyzed the surface expression of each TAM receptor on murine macrophages by flow cytometry. P388D1 cells expressed relatively higher levels of AXL and lower levels of MERTK but no TYRO3, whereas J774 cells expressed MERTK only (Fig. S1). Then, we treated P388D1 and J774 cells with GAS6, a high-affinity ligand for all TAM receptors, for 24 h.<sup>9</sup> To observe autophagy induction, we expressed a tandem fusion of MAP1LC3B (microtubule associated protein 1 light chain 3  $\beta$ ) protein to acid-insensitive mCherry together with GFP (mCherry-EGFP-MAP1LC3B) in these cells, and then performed morphometric analyses using confocal microscopy to monitor the formation of autophagosomes and autolysosomes.<sup>21</sup> In these analyses, autophagosomes were observable as yellow puncta (colocalization between mCherry and GFP) and autolysosomes appeared as red puncta (mCherry).<sup>21</sup> Also, we measured the ratio of MAP1LC3B-I to MAP1LC3B-II because the conversion of MAP1LC3B-I to MAP1LC3B-II is correlated with the formation of autophagosomes.<sup>21,22</sup> The number of yellow puncta and red puncta per cell increased only in GAS6-treated P388D1 cells (Fig. S2A). In agreement with this observation, GAS6-treated P388D1 cells showed increased conversion of MAP1LC3B-I to MAP1LC3B-II relative to untreated cells, whereas GAS6-treated J774 cells did not (Fig. S2B). This result was confirmed by treating P388D1 cells with various concentrations of GAS6 for 24 h. Autophagy was induced in GAS6-treated P388D1 cells in a dose-dependent manner (Fig. 1A and B).

We further tested whether the degree of autophagy induction with GAS6 treatment in macrophages is augmented by

treatment with chloroquine (CQ, a lysosomal acidification inhibitor) or serum deprivation.<sup>21</sup> The results indicated that treatment with CQ and GAS6 increased the level of endogenous MAP1LC3B-II in macrophages, relative to treatment with GAS6 alone or CQ alone (Fig. S2C). However, serum deprivation along with GAS6 treatment had no additive effect on autophagy induction, compared with serum depleted cells (Fig. S2D).

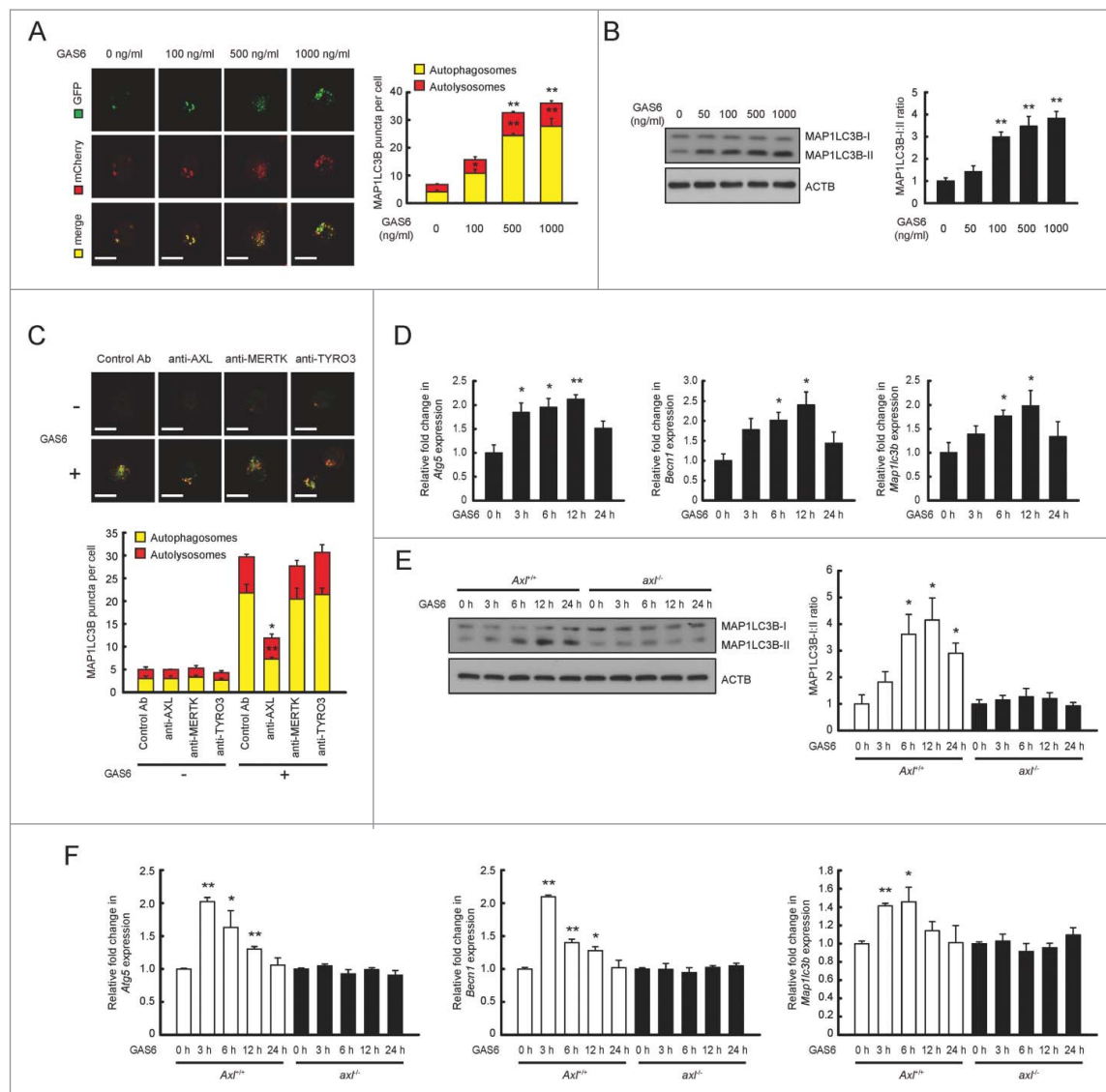
Next, we treated P388D1 cells with neutralizing antibodies against AXL, MERTK, or TYRO3 during GAS6 incubation. Our results indicated that blocking GAS6-AXL signaling abolished autophagy induction in macrophages after GAS6 treatment (Fig. 1C and Fig. S3). ATG5 (Autophagy related 5), BECN1 (Beclin 1) and MAP1LC3B proteins are essential for induction of autophagy.<sup>23</sup> Therefore, we monitored the corresponding mRNA transcripts by qRT-PCR after treatment of P388D1 cells with GAS6. The expression levels of all of these transcripts increased within 24 h after GAS6 treatment (Fig. 1D).

Autophagy induction via GAS6-AXL signaling was further confirmed in wild-type (*Axl*<sup>+/+</sup>) and *axl*<sup>−/−</sup> mice. Surface expression of AXL was confirmed on *Axl*<sup>+/+</sup> macrophages, and was not present on *axl*<sup>−/−</sup> macrophages (Fig. S4). The surface expression levels of MERTK and TYRO3 were not different between *Axl*<sup>+/+</sup> and *axl*<sup>−/−</sup> macrophages (Fig. S4). Upon GAS6 treatment, the conversion of MAP1LC3B-I to MAP1LC3B-II increased in *Axl*<sup>+/+</sup> macrophages, relative to that in untreated cells (Fig. 1E). However, no changes in the MAP1LC3B-I to MAP1LC3B-II ratio were observed in *axl*<sup>−/−</sup> macrophages after GAS6 treatment (Fig. 1E). Also, we monitored mRNA transcripts of *Atg5*, *Becn1* and *Map1lc3b* in GAS6-treated macrophages. Induction of these genes was observed in *Axl*<sup>+/+</sup> macrophages, but not in *axl*<sup>−/−</sup> macrophages following GAS6 treatment (Fig. 1F). Taken together, these results demonstrate that GAS6-AXL signaling mediates autophagy induction by increasing the expression of *Atg5*, *Becn1* and *Map1lc3b* in macrophages.

### Autophosphorylation of 2 tyrosine residues, Tyr815 and Tyr860, in the cytoplasmic domain of AXL is required for autophagy induction

We generated a mutant lacking the entire cytoplasmic domain of AXL (AXL<sup>CYΔ</sup>) (Table S2 and Fig. S5A). Wild-type AXL (WT AXL) or AXL<sup>CYΔ</sup> was expressed in J774 cells which lack endogenous AXL. The expression level of AXL<sup>CYΔ</sup> was comparable to that of WT AXL (Fig. S5B). Then, we treated these cells with GAS6 to test whether the cytoplasmic domain of AXL is required for autophagy induction. WT *Axl* transfectants showed enhanced conversion of MAP1LC3B-I to MAP1LC3B-II after GAS6 treatment, whereas *Axl*<sup>CYΔ</sup> transfectants did not (Fig. 2A). To confirm this observation, we monitored mRNA transcripts of *Atg5*, *Becn1* and *Map1lc3b* in WT *Axl* or *Axl*<sup>CYΔ</sup> transfectants after GAS6 treatment. Expression of these genes was induced only in GAS6-treated WT *Axl* transfectants, and not in GAS6-treated *Axl*<sup>CYΔ</sup> transfectants (Fig. 2B).

Three tyrosine residues (Tyr773, Tyr815, Tyr860) in the cytoplasmic domain of mouse AXL have been identified as potential autophosphorylation sites which mediate signal transduction.<sup>24</sup> To determine which tyrosine residue mediates the

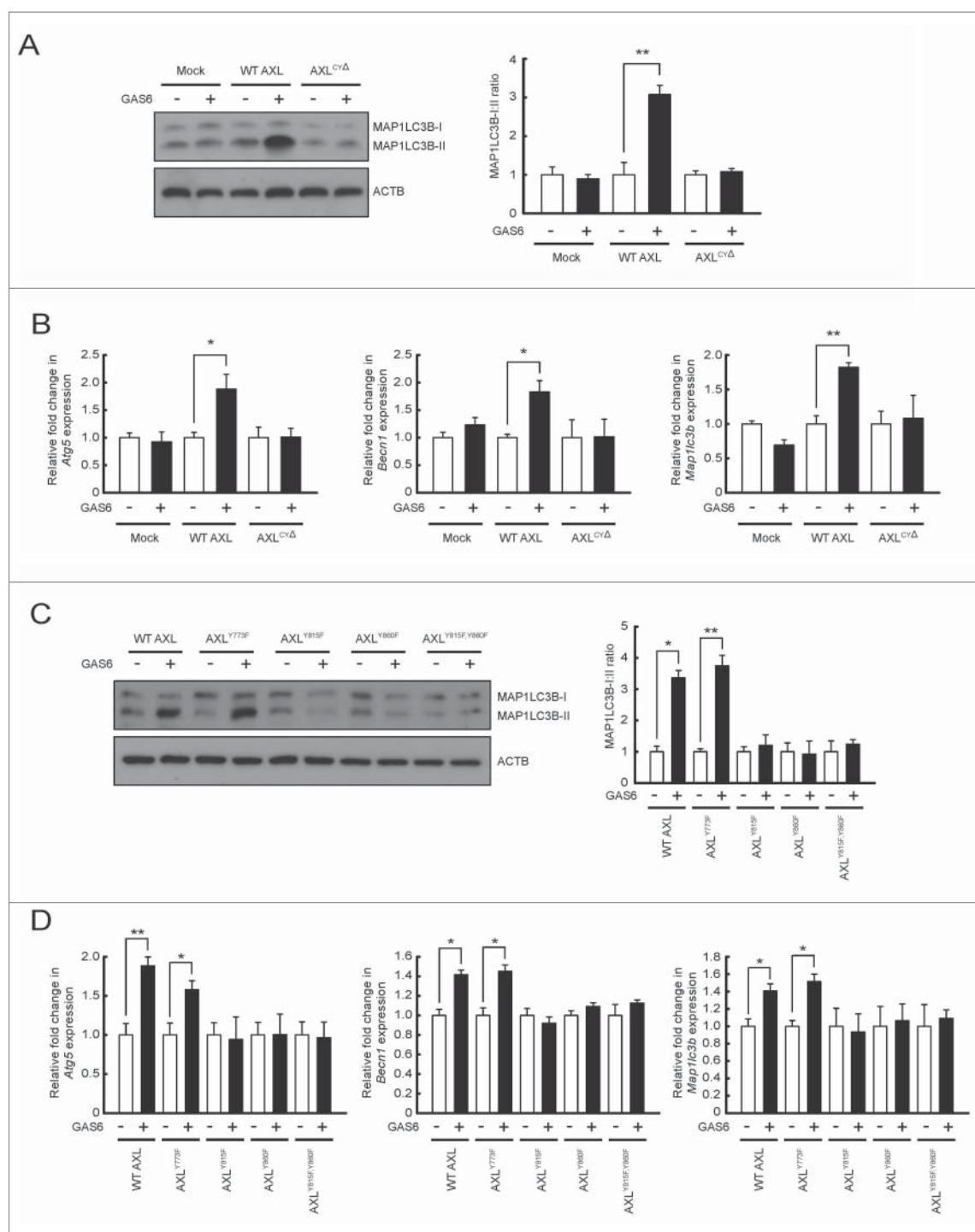


**Figure 1.** Interaction between GAS6 and AXL induces autophagy in macrophages. (A) mCherry-EGFP-MAP1LC3B expressing P388D1 cells were treated with various concentrations of GAS6 for 24 h. After treatment, the formation of autophagosomes (yellow puncta) and autolysosomes (red puncta) was analyzed under a confocal microscope (left panel). Scale bar: 10  $\mu$ m. Quantifications of autophagosome and autolysosome formation are shown in the right panel. (B) P388D1 cells were treated with various concentrations of GAS6 for 24 h. After treatment, cell lysates were subjected to immunoblot analyses using anti-MAP1LC3B antibody and anti-ACTB/actin,  $\beta$  antibody (left panel). The ratios of MAP1LC3B-I to MAP1LC3B-II are shown in the right panel. (C) mCherry-EGFP-MAP1LC3B-expressing P388D1 cells were treated with various TAM neutralizing antibodies in the presence or absence of GAS6 (100 ng/ml) for 24 h. Then, the formation of autophagosomes and autolysosomes was analyzed by confocal microscopy (upper panel). Scale bar: 10  $\mu$ m. Quantifications of autophagosome and autolysosome formation are shown in the lower panel. Control antibody, isotype control; anti-AXL, AXL neutralizing antibody; anti-MERTK, MERTK neutralizing antibody; anti-TYRO3, TYRO3 neutralizing antibody; “–”, no treatment; “+”, treatment. (D) P388D1 cells were treated with GAS6 (100 ng/ml) for the indicated times. After treatment, qRT-PCR was performed using mRNA from each cell as a template. (E and F) Peritoneal macrophages isolated from *Axl*<sup>+/+</sup> and *Axl*<sup>-/-</sup> mice were treated with GAS6 (100 ng/ml) for the indicated times. After treatment, cell lysates were subjected to immunoblot analyses (E, left panel). The ratios of MAP1LC3B-I to MAP1LC3B-II are shown (E, right panel). Also, qRT-PCR was performed using mRNA from each cell as a template (F). *Axl*<sup>+/+</sup>, *Axl*<sup>+/+</sup> peritoneal macrophages; *Axl*<sup>-/-</sup>, *Axl*<sup>-/-</sup> peritoneal macrophages. All data represent the mean  $\pm$  SEM from 3 independent experiments. \**P* < 0.05; \*\**P* < 0.01.

signal for autophagy induction, we made several mutants with amino acid substitutions (AXL<sup>Y773F</sup> replaces Tyr773 with Phe773, AXL<sup>Y815F</sup> replaces Tyr815 with Phe815 and AXL<sup>Y860F</sup> replaces Tyr860 with Phe860) (Table S2 and Fig. S5A). After verifying the proper cell surface expression of each mutant protein on J774 cells (Fig. S5B), we compared the extent of autophagy induction of each mutant transfectant with that of the WT *Axl* transfectant after GAS6 treatment. The conversion of MAP1LC3B-I to MAP1LC3B-II in GAS6-treated WT *Axl* and *Axl*<sup>Y773F</sup> (Tyr773 to Phe773) transfectants was increased relative to that in untreated cells, whereas the conversion of MAP1LC3B-I to MAP1LC3B-II in *Axl*<sup>Y815F</sup> (Tyr815 to

Phe815) and *Axl*<sup>Y860F</sup> (Tyr860 to Phe860) transfectants was not (Fig. 2C). To confirm this result, we monitored mRNA levels of *Atg5*, *Becn1* and *Map1lc3b* in each transfectant after GAS6 treatment. These genes were induced in WT *Axl* and *Axl*<sup>Y773F</sup> transfectants, but not in *Axl*<sup>Y815F</sup> and *Axl*<sup>Y860F</sup> transfectants (Fig. 2D).

To further verify that Tyr815 and Tyr860 residues are important for autophagy induction via GAS6-AXL signaling, we also made a double amino acid substitution mutant (AXL<sup>Y815F,Y860F</sup> replaces Tyr815 and Tyr860 with Phe815 and Phe860 respectively) (Table S2 and Fig. S5A and B) and tested whether this mutant is capable of autophagy induction after



**Figure 2.** Two autophosphorylation residues (Tyr815 and Tyr860) within the cytoplasmic domain of AXL are required for autophagy induction through GAS6-AXL signaling. (A and B) Wild-type AXL (WT AXL) and its cytoplasmic domain deletion mutant (AXL<sup>Δ</sup>) were expressed in J774 cells. Then, the transfected cells were treated with GAS6 (100 ng/ml) for 24 h. After treatment, cell lysates were subjected to immunoblot analyses using anti-MAP1LC3B antibody and anti-ACTB antibody (A, left panel). The ratios of MAP1LC3B-I to MAP1LC3B-II are shown (A, right panel). Also, qRT-PCR was performed using mRNA from each cell as a template (B). “–”, no treatment; “+”, treatment; Mock, empty vector transfectant. (C and D) Wild-type AXL (WT AXL) and several AXL mutants were expressed in J774 cells. Then, transfected cells were treated with GAS6 (100 ng/ml) for 24 h. After treatment, cell lysates were subjected to immunoblot analyses (C, left panel). The ratios of MAP1LC3B-I to MAP1LC3B-II are shown (C, right panel). Also, qRT-PCR was performed using mRNA from each cell as a template (D). AXL<sup>Y773F</sup>, AXL mutant with Tyr773 to Phe773; AXL<sup>Y815F</sup>, AXL mutant with Tyr815 to Phe815; AXL<sup>Y860F</sup>, AXL mutant with Tyr860 to Phe860; and AXL<sup>Y815F,Y860F</sup>, AXL double mutant with Tyr815 and Tyr860 to Phe815 and Phe860 respectively. “–”, no treatment; “+”, treatment. All data represent the mean ± SEM from 3 independent experiments. \**P* < 0.05; \*\**P* < 0.01.

GAS6 treatment. The results clearly demonstrated that the conversion of MAP1LC3B-I to MAP1LC3B-II and the mRNA levels of *Atg5*, *Becl1* and *Map1lc3b* were not different in the GAS6-treated Axl<sup>Y815F,Y860F</sup> transfectant than in untreated cells (Fig. 2C and D).

### Blocking the MAPK14 pathway inhibits AXL-mediated autophagy induction in macrophages

We tested several different kinase inhibitors to identify those that would block downstream effectors of GAS6-AXL



signaling in order to determine which downstream pathway is involved in autophagy induction. After treatment of GAS6 with several kinase inhibitors in J774 cells expressing WT *Axl*, the extent of autophagy induction was measured by monitoring the conversion from MAP1LC3B-I to MAP1LC3B-II after GAS6 treatment. In these experiments, we also assessed the formation of autophagosomes and autolysosomes by detecting fluorescence puncta in WT *Axl* expressing mCherry-EGFP-MAP1LC3B. As expected, no autophagy induction was observed in cells after treatment with R428 (AXL inhibitor) and GAS6 (Fig. 3A and B, and Fig. S6). However, treatment with U0126 (MAP2K1/2 [mitogen-activated protein kinase 1/2] and MAPK1/3 inhibitor), SP600125 (MAPK8/9/10 inhibitor), BKM120 (PtdIns3K inhibitor) and rapamycin (MTOR [mechanistic target of rapamycin] inhibitor) had no effect on autophagy induction through GAS6-AXL signaling (Fig. 3A and B and Fig. S6). Notably, treatment with SB203580 (MAPK11/14 inhibitor) abolished GAS6-AXL-mediated autophagy induction (Fig. 3A and B and Fig. S6). In support of this result, *Atg5*, *Becn1* and *Map1lc3b* mRNA levels were not increased in cells treated with R428 or SB203580 together with GAS6, whereas they were increased in cells treated with U0126, SP600125, BKM120, or rapamycin along with GAS6 (Fig. 3C).

Since SB203580 inhibits both MAPK11 and MAPK14 activities,<sup>25</sup> we monitored mRNA transcripts of *Mapk11* and *Mapk14* in AXL-expressing J774 cells before or after treatment with GAS6. The mRNA transcript of *Mapk14* was observed whereas mRNA transcript of *Mapk11* was hardly detected in AXL-expressing J774 cells by RT-PCR analyses (Fig. S7A). Further, we analyzed the activation status of MAPK11 or MAPK14 using an activation-specific anti-phospho MAPK antibody in AXL-expressing J774 cells after treatment with GAS6 and SB203580. MAPK14 activation in AXL-expressing J774 cells was successfully blocked by treating SB203580 in a dose-dependent manner. However, no activation form of MAPK11 was detected in AXL-expressing J774 cells (Fig. S7B).

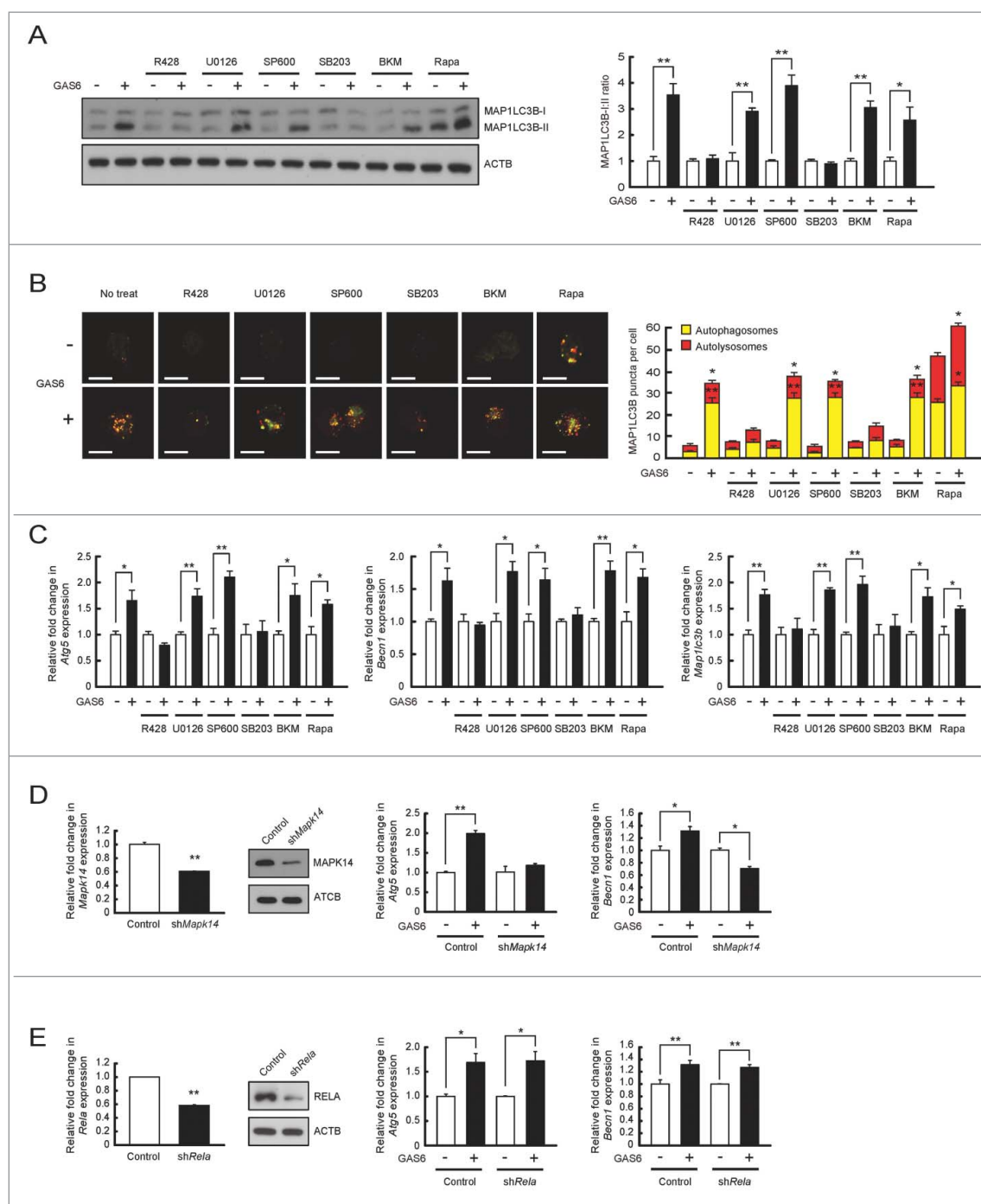
To confirm these results, we depleted MAPK14 in AXL-expressing J774 cells using shRNA and monitored mRNA transcripts of *Atg5* and *Becn1* after GAS6 treatment. The levels of MAPK14 expression were significantly decreased in the sh*Mapk14* plasmid transfectant (sh*Mapk14*) when compared to levels in the control plasmid transfectant (control) (Fig. 3D). Moreover, shRNA-mediated knockdown of MAPK14 clearly abolished the upregulation of *Atg5* and *Becn1* mRNA transcripts after GAS6 treatment (Fig. 3D). Together, these results indicate that GAS6-AXL signaling mediated autophagy induction is dependent on the activity of MAPK14.

To rule out the possibility that NFκB (nuclear factor of kappa light polypeptide gene enhancer in B cells) is involved in GAS6-AXL-mediated autophagy induction, we also depleted *Rela* (v-rel avian reticuloendotheliosis viral oncogene homolog A), a key subunit of NFκB, in AXL-expressing J774 cells, using shRNA and measured the expression patterns of *Atg5* and *Becn1* after GAS6 treatment. The shRNA-mediated knockdown of *Rela* did not change the expression levels of *Atg5* and *Becn1* mRNA transcripts after GAS6 treatment (Fig. 3E).

### Autophagy induction by GAS6-AXL signaling mediates suppression of IL1B and IL18 production by inhibiting NLRP3 inflammasome activation

To evaluate whether autophagy induction by GAS6-AXL signaling inhibits NLRP3 inflammasome activation in murine macrophages, we pretreated *Axl*<sup>+/+</sup> or *axl*<sup>-/-</sup> macrophages with LPS and GAS6, and then treated them with ATP, a well-characterized NLRP3 stimulator.<sup>26,27</sup>

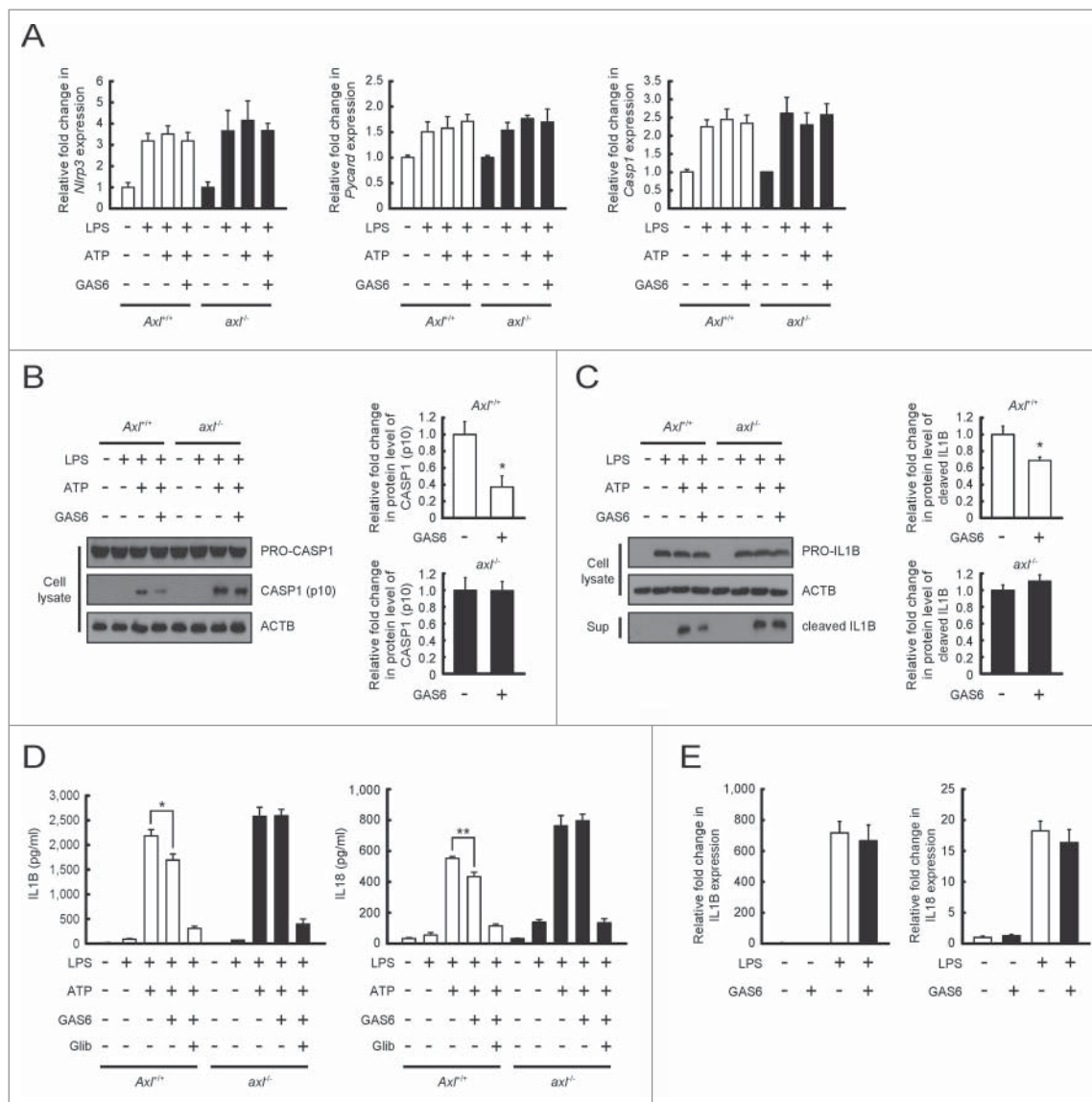
After NLRP3 inflammasome activation, the levels of *Nlrp3*, *Pycard* (PYD and CARD domain containing), and *Casp1* mRNA transcripts were increased in both *Axl*<sup>+/+</sup> and *axl*<sup>-/-</sup> macrophages. No significant change in the mRNA levels of these inflammasome components was observed between *Axl*<sup>+/+</sup> and *axl*<sup>-/-</sup> macrophages regardless of the presence or absence of GAS6 (Fig. 4A). Interestingly, GAS6-treated *Axl*<sup>+/+</sup> macrophages were found to have reduced levels of cleaved CASP1 (p10, the active form of CASP1) compared to untreated *Axl*<sup>+/+</sup> macrophages (Fig. 4B). However, GAS6-treated *axl*<sup>-/-</sup> macrophages exhibited no change in the active form of CASP1 relative to untreated *axl*<sup>-/-</sup> macrophages (Fig. 4B). Consistent with these results, GAS6-treated *Axl*<sup>+/+</sup> macrophages had reduced levels of the cleaved form of IL1B, which is produced from a precursor (PRO-IL1B) by activated CASP1, in response to treatment with LPS and ATP than did untreated *Axl*<sup>+/+</sup> macrophages (Fig. 4C). However, GAS6-treated *axl*<sup>-/-</sup> macrophages and untreated *axl*<sup>-/-</sup> macrophages had comparable levels of the cleaved form of IL1B (Fig. 4C). These findings were further confirmed by ELISA results showing decreases in IL1B and IL18 secretion in GAS6-treated *Axl*<sup>+/+</sup> macrophages compared with untreated *Axl*<sup>+/+</sup> macrophages (Fig. 4D). As expected, no significant changes were observed in the secretion of these proinflammatory cytokines in GAS6-treated or untreated *axl*<sup>-/-</sup> macrophages (Fig. 4D). In addition, glibenclamide (NLRP3 inflammasome inhibitor)<sup>18</sup> treatment effectively blocked secretion of IL1B and IL18 from macrophages treated with LPS and ATP (Fig. 4D). After activation of the NLRP3 inflammasome, we measured mRNA transcripts of *Il1b* and *Il18* by qRT-PCR to determine whether treatment of macrophages with GAS6 affects the expression of these genes. The levels of *Il1b* and *Il18* mRNA transcripts in both *Axl*<sup>+/+</sup> and *axl*<sup>-/-</sup> macrophages were not altered by treatment with GAS6 (Fig. 4E). To confirm these results, we pretreated *Atg7*<sup>fl/fl</sup> *Lyz2-Cre*<sup>+</sup> (*Atg7*<sup>fl/fl</sup> CKO) or *Atg7*<sup>fl/fl</sup> *Lyz2-Cre*<sup>-</sup> (*Atg7*<sup>fl/fl</sup> CTRL) macrophages<sup>28,29</sup> with LPS and GAS6, and then treated them with ATP. The results demonstrated that *Atg7*<sup>fl/fl</sup> CKO macrophages were defective in conversion of MAP1LC3B-I to MAP1LC3B-II after GAS6 treatment, whereas increased endogenous MAP1LC3B-II levels were found in *Atg7*<sup>fl/fl</sup> CTRL macrophages after GAS6 treatment (Fig. S8A). This result indicates that selective deletion of *Atg7* in macrophages causes a defect in autophagy induction after GAS6 treatment. Furthermore, GAS6-treated *Atg7*<sup>fl/fl</sup> CKO macrophages had no changes in the active form of CASP1 and the cleaved form of IL1B relative to untreated *Atg7*<sup>fl/fl</sup> CKO macrophages (Fig. S8B and C). In contrast to the results from *Atg7*<sup>fl/fl</sup> CTRL macrophages, GAS6-treated *Atg7*<sup>fl/fl</sup> CTRL macrophages were found to have reduced levels of the active form of CASP1 and the cleaved form of IL1B relative to untreated *Atg7*<sup>fl/fl</sup> CTRL macrophages (Fig. S8B and C). Supporting these results, levels of IL1B and IL18 secreted



**Figure 3.** Inhibition of the MAPK14 pathway blocks GAS6-AXL signaling-mediated autophagy induction. (A to C) J774 cells expressing WT AXL or WT AXL and mCherry-EGFP-MAP1LC3B were treated with GAS6 (100 ng/ml) in the absence or presence of various kinase inhibitors for 24 h. After treatment, cell lysates were subjected to immunoblot analyses using anti-MAP1LC3B antibody and anti-ACTB antibody (A, left panel). The ratios of MAP1LC3B-I to MAP1LC3B-II are shown (A, right panel). Then, the formation of autophagosomes (yellow puncta) and autolysosomes (red puncta) was analyzed by confocal microscopy (B, left panel). Scale bar: 10  $\mu$ m. Quantifications of autophagosome and autolysosome formation are shown in the right panel (B, right panel). Also, qRT-PCR was performed using mRNA from each cell as a template (C). R428, AXL inhibitor; U0126, MAP2K1/2 and MAPK1/3 inhibitor; SP600 (SP600125), MAPK8/9/10 inhibitor; SB203 (SB203580), MAPK11/14 inhibitor; BKM (BKM120), PtdIns3K inhibitor; Rapa (rapamycin), MTOR inhibitor; “–”, no treatment; “+”, treatment. (D) Control plasmid (Control) and *shMapk14* plasmid (*shMapk14*) were transfected into WT AXL-expressing J774 cells. Then, qRT-PCR and immunoblot analyses were performed to measure the level of MAPK14 expression (left panel). After treatment with GAS6 (100 ng/ml) for 24 h, qRT-PCR was performed to detect *Atg5* and *Beclin1* mRNA transcripts (right panel). “–”, no treatment; “+”, treatment. (E) Control plasmid (Control) and *shRela* plasmid (*shRela*) were transfected into WT AXL-expressing J774 cells. Then, qRT-PCR and immunoblot analyses were performed to measure the level of RELA expression (left panel). After treatment with GAS6 (100 ng/ml) for 24 h, qRT-PCR was performed to detect *Atg5* and *Beclin1* mRNA transcripts (right panel). “–”, no treatment; “+”, treatment. All data represent the mean  $\pm$  SEM from 3 independent experiments. \* $P < 0.05$ ; \*\* $P < 0.01$ .

from GAS6-treated *Atg7<sup>fl/fl</sup>* CKO macrophages were the same as those from untreated *Atg7<sup>fl/fl</sup>* CKO macrophages, whereas the extent of IL1B and IL18 secretion from GAS6-treated *Atg7<sup>fl/fl</sup>* CTRL macrophages was significantly decreased (Fig. S8D).

Collectively, these data strongly suggest that GAS6-AXL signaling-mediated autophagy induction inhibits the conversion of the active forms of IL1B and IL18 through NLRP3 inflammasome-mediated activation of CASP1.



**Figure 4.** Autophagy induction through GAS6-AXL signaling reduces IL1B and IL18 secretion by inhibiting NLRP3 inflammasome-mediated CASP1 activation. (A to D) Peritoneal macrophages isolated from *Ax1*<sup>+/+</sup> and *ax1*<sup>-/-</sup> mice were treated with LPS (100 ng/ml) for 6 h and then stimulated with ATP (5 mM) in the absence or presence of GAS6 (100 ng/ml) or NLRP3 inflammasome inhibitor (Glib, 100  $\mu$ M). After treatment, qRT-PCR was performed using mRNA from each cell as a template (A). Also, cell lysates or culture supernatants were subjected to immunoblot analyses using anti-CASP1 antibody (B) and anti-IL1B antibody (C). Anti-ACTB antibody was used as an internal control for immunoblotting. Then, ELISAs were performed to detect IL1B and IL18 secretions in culture supernatants (D). “—”, no treatment; “+”, treatment; *Ax1*<sup>+/+</sup>, *Ax1*<sup>+/+</sup> peritoneal macrophages; *ax1*<sup>-/-</sup>, *ax1*<sup>-/-</sup> peritoneal macrophages; Sup, culture supernatant; Glib, Glibenclamide. (E) Peritoneal macrophages isolated from *Ax1*<sup>+/+</sup> mice were treated with LPS (100 ng/ml) for 6 h in the absence or presence of GAS6 (100 ng/ml). After treatment, qRT-PCR was performed using mRNA from each cell as a template. All data represent the mean  $\pm$  SEM from 3 independent experiments. \**P* < 0.05; \*\**P* < 0.01.

Previous observations demonstrated that STAT1 (signal transducer and activator of transcription 1)-dependent type I IFN (interferon) signaling suppresses CASP1 dependent IL1B maturation by repressing NLRP3 inflammasome activation.<sup>30</sup> To determine whether NLRP3 inflammasome inhibition through GAS6-AXL signaling is dependent on the activity of type I IFN and STAT1, we blocked type I IFN signaling using an anti-IFNAR1 (interferon  $\alpha$  and  $\beta$  receptor subunit 1) antibody (5A3 clone) and measured the degree of NLRP3 inflammasome activation in *Ax1*<sup>+/+</sup> and *ax1*<sup>-/-</sup> macrophages. After treatment with anti-IFNAR1 antibody, phosphorylation of STAT1 (p-STAT1) was decreased in a dose-dependent manner in LPS-activated macrophages (Fig. S9A). Then, we activated NLRP3 inflammasomes in *Ax1*<sup>+/+</sup> and *ax1*<sup>-/-</sup> macrophages by treatment with an anti-IFNAR1 antibody and GAS6. Our

results indicated that treatment with the anti-IFNAR1 antibody during NLRP3 inflammasome activation did not change the conversion of PRO-IL1B to mature IL1B in GAS6-treated *Ax1*<sup>+/+</sup> or *ax1*<sup>-/-</sup> macrophages (Fig. S9B). Consistent with this result, the decrease in IL1B secretion is dependent on GAS6-AXL signaling, but not on type I IFN signaling (Fig. S9C).

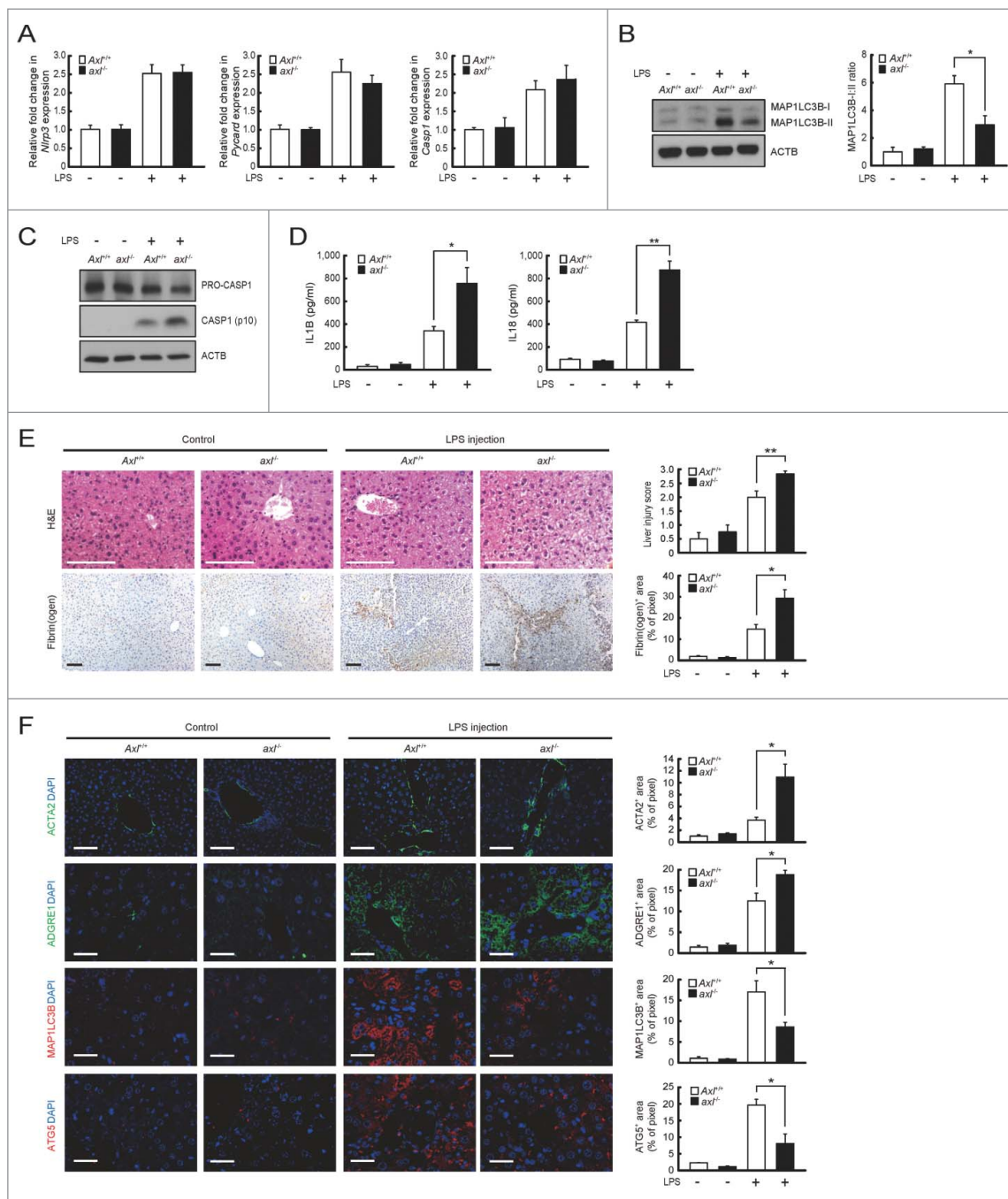
#### **GAS6-AXL signaling-mediated autophagy induction in Kupffer cells ameliorates acute liver injury by inhibition of NLRP3 inflammasome activation**

Since recent observations demonstrated that NLRP3 inflammasome activation in Kupffer cells contributes to severe liver inflammation,<sup>31,32</sup> we investigated whether *ax1*<sup>-/-</sup> mice aggravate the symptom of acute liver inflammation induced by LPS



or  $\text{CCl}_4$ . *Gas6* mRNA levels were increased in liver and spleen tissues within 12 h after LPS treatment (Fig. S10). Similarly, the levels of *Nlrp3*, *Pycard* and *Casp1* mRNA transcripts were significantly increased in both  $\text{Axl}^{+/+}$  and  $\text{axl}^{-/-}$  Kupffer cells within 12 h after LPS treatment (Fig. 5A). These results indicate that LPS treatment leads to the induction of *Gas6* and the

activation of NLRP3 inflammasomes in Kupffer cells. After treatment with LPS, the conversion of MAP1LC3B-I to MAP1LC3B-II in  $\text{Axl}^{+/+}$  Kupffer cells was significantly increased relative to that in  $\text{axl}^{-/-}$  Kupffer cells (Fig. 5B). Consequently, LPS-treated  $\text{Axl}^{+/+}$  Kupffer cells contained the less active form of CASP1 (p10), whereas LPS-treated  $\text{axl}^{-/-}$



**Figure 5.** *Axl* deficiency in mice aggravates hepatic inflammation after LPS challenge.  $\text{Axl}^{+/+}$  and  $\text{axl}^{-/-}$  mice were injected intraperitoneally with vehicle (saline, Control) or LPS (2.5  $\mu\text{g/g}$ ). Mice were sacrificed and analyzed 12 h after treatment. (A) qRT-PCR was performed using mRNA from  $\text{Axl}^{+/+}$  or  $\text{axl}^{-/-}$  Kupffer cells ( $\text{Axl}^{+/+}$  or  $\text{axl}^{-/-}$ ) as templates. (B) Cell lysates from  $\text{Axl}^{+/+}$  or  $\text{axl}^{-/-}$  Kupffer cells were subjected to immunoblot analyses using anti-MAP1LC3B antibody and anti-ACTB antibody (left panel). The ratios of MAP1LC3B-I to MAP1LC3B-II are shown (right panel). (C) Cell lysates from  $\text{Axl}^{+/+}$  or  $\text{axl}^{-/-}$  Kupffer cells were subjected to immunoblot analyses using anti-CASP1 antibody and anti-ACTB antibody. (D) ELISAs were performed to detect serum concentrations of IL1B and IL18 from  $\text{Axl}^{+/+}$  or  $\text{axl}^{-/-}$  mice ( $\text{Axl}^{+/+}$  or  $\text{axl}^{-/-}$ ). (E) Hematoxylin and eosin (H&E) staining of liver sections (upper left) and liver injury scores (upper right) from  $\text{Axl}^{+/+}$  or  $\text{axl}^{-/-}$  mice are shown in the upper panel. Immunohistochemistry of liver sections with anti-fibrin(ogen) antibody (lower left) and fibrin(ogen) deposition area (lower right) from  $\text{Axl}^{+/+}$  or  $\text{axl}^{-/-}$  mice are shown in the lower panel. Fibrin(ogen) deposition area = stained area/total image area. Scale bar: 100  $\mu\text{m}$ . (F) Immunohistochemistry of liver sections with anti-ACTA2 antibody, anti-ADGRE1/F4/80 antibody (ADGRE1), anti-MAP1LC3B antibody (MAP1LC3B) and anti-ATG5 antibody (ATG5) from  $\text{Axl}^{+/+}$  or  $\text{axl}^{-/-}$  mice. Each staining area = stained area/total image area. DAPI staining was performed to visualize nuclei. Scale bar: 100  $\mu\text{m}$ . “-”, vehicle treatment; “+”, LPS treatment. All data represent the mean  $\pm$  SEM from 3 independent experiments. \* $P < 0.05$ ; \*\* $P < 0.01$ .



kupffer cells did not (Fig. 5C). Consistent with these results, IL1B and IL18 secretions in sera taken from LPS-treated *Axl*<sup>+/+</sup> mice were significantly decreased compared with those in sera from LPS-treated *axl*<sup>-/-</sup> mice (Fig. 5D). However, the levels of *Il1b* and *Il18* mRNA transcripts in *Axl*<sup>+/+</sup> and *axl*<sup>-/-</sup> Kupffer cells were comparable (Fig. S11).

To confirm that NLRP3 inflammasome activation is involved in the increased inflammation seen in *axl*<sup>-/-</sup> mice, we used glibenclamide to inhibit NLRP3 inflammasome activation in this animal model.<sup>33</sup> The results showed that glibenclamide treatment diminished the active form of CASP1 (p10) in both LPS-treated *Axl*<sup>+/+</sup> and *axl*<sup>-/-</sup> Kupffer cells (Fig. S12A). Also, glibenclamide treatment caused a significant decrease in IL1B and IL18 levels in sera taken from LPS-treated *Axl*<sup>+/+</sup> or *axl*<sup>-/-</sup> mice (Fig. S12B).

Liver tissue specimens from *Axl*<sup>+/+</sup> and *axl*<sup>-/-</sup> mice were obtained 12 h after LPS treatment. Normal histology was observed in the control groups without treatment (Fig. 5E, upper panels). In contrast, marked histological changes (multiple erosions, inflammatory cell infiltration and bleeding) were observed in the LPS-treated groups (Fig. 5E, upper panels). More severe tissue injury was observed in the LPS-treated *axl*<sup>-/-</sup> group than in the *Axl*<sup>+/+</sup> group. Accordingly, liver injury score was higher in specimens from the LPS-treated *axl*<sup>-/-</sup> mouse group than in those from the LPS-treated *Axl*<sup>+/+</sup> mouse group (Fig. 5E, upper panels). Consistent with this, more severe kidney and lung tissue injury was also observed in LPS-treated *axl*<sup>-/-</sup> mice compared with *Axl*<sup>+/+</sup> mice (Fig. S13).

The degree of fibrin deposition in the liver is a useful indicator of measuring the severity of acute liver injury.<sup>34</sup> The amount of fibrin deposition in LPS-treated *axl*<sup>-/-</sup> mice was significantly greater than in *Axl*<sup>+/+</sup> mice (Fig. 5E, lower panels). In order to access the severity of liver injury, we also measured hepatic stellate cell (HSC) activation by staining with anti-ACTA2 (actin,  $\alpha$  2, smooth muscle, aorta) antibody (green fluorescence) and visualized the number of macrophages within the lesions by staining with anti-ADGRE1/F4/80 antibody (red fluorescence).<sup>35</sup> The results showed that activated HSCs and infiltrated macrophages at the sites of injury were more numerous in the livers of LPS-treated *axl*<sup>-/-</sup> mice than in those of *Axl*<sup>+/+</sup> mice (Fig. 5F, upper 2 panels).

The combined results indicate that *axl*<sup>-/-</sup> mice show more severe inflammation following LPS-induced liver injury because *axl*<sup>-/-</sup> mice cannot inhibit NLRP3 inflammasome activation due to deficits in GAS6-AXL signaling-mediated autophagy induction. Supporting this idea, immunohistochemical staining with anti-MAP1LC3B antibody and anti-ATG5 antibody showed that the number of cells expressing MAP1LC3B and ATG5 proteins was markedly elevated in liver tissue from LPS-treated *Axl*<sup>+/+</sup> mice compared with that from LPS-treated *axl*<sup>-/-</sup> mice (Fig. 5F, lower 2 panels).<sup>36,37</sup> The liver function of experimental animals was further determined by measuring serum levels of GPT (glutamic pyruvic transaminase, soluble) and GOT1 (glutamic-oxaloacetic transaminase 1, soluble). Serum levels of GPT and GOT1 were more elevated in the LPS-treated *axl*<sup>-/-</sup> group than in the LPS-treated *Axl*<sup>+/+</sup> group (Fig. S14).

Using a more liver-specific injury model to evaluate the inhibitory effect of GAS6-AXL signaling on NLRP3

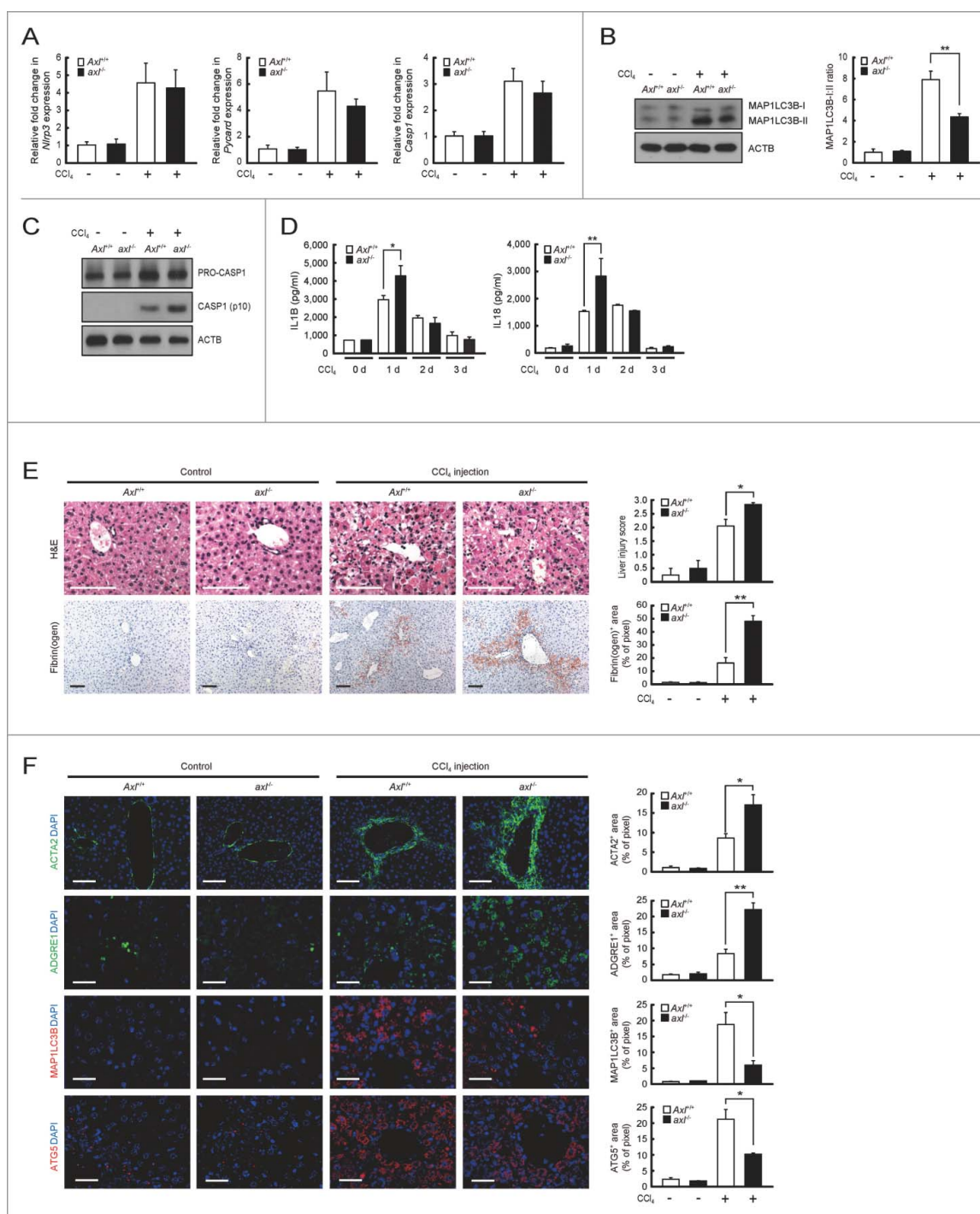
inflammasome activation, we performed the same sets of experiments in mice subjected to intraperitoneal injections of either CCl<sub>4</sub> or vehicle. *Gas6* mRNA transcript levels increased in liver tissue of CCl<sub>4</sub>-treated animals 24 h after treatment (Fig. S15). Also, *Nlrp3*, *Pycard* and *Casp1* mRNA levels were elevated in *Axl*<sup>+/+</sup> and *axl*<sup>-/-</sup> Kupffer cells 24 h after CCl<sub>4</sub> treatment (Fig. 6A). The conversion of MAP1LC3B-I to MAP1LC3B-II in *Axl*<sup>+/+</sup> Kupffer cells was significantly increased relative to that in *axl*<sup>-/-</sup> Kupffer cells following treatment with CCl<sub>4</sub> (Fig. 6B). Consequently, Kupffer cells from CCl<sub>4</sub>-treated *Axl*<sup>+/+</sup> mice expressed the less active form of CASP1 (p10), whereas *axl*<sup>-/-</sup> Kupffer cells from CCl<sub>4</sub>-treated mice did not (Fig. 6C). Supporting this result, IL1B and IL18 secretions 24 h after CCl<sub>4</sub> treatment were significantly decreased in sera from *Axl*<sup>+/+</sup> mice, compared with that from *axl*<sup>-/-</sup> mice (Fig. 6D). However, the levels of *Il1b* and *Il18* mRNA transcripts in *Axl*<sup>+/+</sup> and *axl*<sup>-/-</sup> Kupffer cells were not significantly different (Fig. S16).

To investigate whether NLRP3 inflammasome activation participates in the increased inflammation observed in *axl*<sup>-/-</sup> mice, we used glibenclamide to inhibit the activation of NLRP3 inflammasome in this animal model.<sup>32</sup> Glibenclamide treatment in both CCl<sub>4</sub>-treated *Axl*<sup>+/+</sup> and *axl*<sup>-/-</sup> Kupffer cells led to decreased conversion of active CASP1 (p10) (Fig. S17A). Also, the amounts of IL1B and IL18 in sera taken from CCl<sub>4</sub>-treated *Axl*<sup>+/+</sup> and *axl*<sup>-/-</sup> mice were significantly reduced by glibenclamide treatment (Fig. S17B).<sup>33</sup>

Liver tissue specimens from *axl*<sup>-/-</sup> and *Axl*<sup>+/+</sup> mice were collected 2 d after CCl<sub>4</sub> treatment. Specimens from the CCl<sub>4</sub>-treated *axl*<sup>-/-</sup> group had higher liver injury scores and a higher degree of fibrin deposition than did those from the CCl<sub>4</sub>-treated *Axl*<sup>+/+</sup> group (Fig. 6E). In agreement with these observations, infiltration of activated HSCs and ADGRE1-positive macrophages into injury sites was increased in livers from CCl<sub>4</sub>-treated *axl*<sup>-/-</sup> mice than in those of CCl<sub>4</sub>-treated *Axl*<sup>+/+</sup> mice (Fig. 6F, upper 2 panels). Also, the number of cells expressing MAP1LC3B and ATG5 proteins was elevated in livers from CCl<sub>4</sub>-treated *Axl*<sup>+/+</sup> mice compared with those from CCl<sub>4</sub>-treated *axl*<sup>-/-</sup> mice (Fig. 6F, lower 2 panels), and serum levels of GPT and GOT1 on d 2 post-CCl<sub>4</sub> treatment were statistically higher in CCl<sub>4</sub>-treated *axl*<sup>-/-</sup> mice than in CCl<sub>4</sub>-treated *Axl*<sup>+/+</sup> mice (Fig. S18). These combined results are consistent with the result from the LPS-induced liver injury model and demonstrate that GAS6-AXL signaling inhibits NLRP3 inflammasome activation through autophagy induction following CCl<sub>4</sub>-induced liver injury.

## Discussion

This study provides novel evidence showing that GAS6-AXL signaling promotes autophagy induction in murine macrophages, which may depress acute liver inflammation by inhibiting NLRP3 inflammasome activation. Based on our study, AXL is the only molecule that induces autophagy among TAM receptors. This result was further confirmed by the observation that mRNA expression levels of *Atg5*, *Becn1* and *Map1lc3b*, essential genes for autophagy induction,<sup>23</sup> increased when we triggered GAS6-AXL signaling. Consistent with this observation, autophagy induction via GAS6-AXL signaling was found to be defective in *axl*<sup>-/-</sup> macrophages.



**Figure 6.** *Axl*-deficient mice display more severe hepatic inflammation after CCl<sub>4</sub> treatment. *Axl*<sup>+/+</sup> and *Axl*<sup>-/-</sup> mice were injected intraperitoneally with vehicle (corn oil, Control) or CCl<sub>4</sub> (2  $\mu$ l/g). Mice were sacrificed and analyzed 2 d after treatment. (A) qRT-PCR was performed using mRNA from *Axl*<sup>+/+</sup> or *Axl*<sup>-/-</sup> Kupffer cells (*Axl*<sup>+/+</sup> or *Axl*<sup>-/-</sup>) as templates. (B) Cell lysates from *Axl*<sup>+/+</sup> or *Axl*<sup>-/-</sup> Kupffer cells were subjected to immunoblot analyses using anti-MAP1LC3B antibody and anti-ACTB antibody (left panel). The ratios of MAP1LC3B-I to MAP1LC3B-II are shown (right panel). (C) Cell lysates from *Axl*<sup>+/+</sup> or *Axl*<sup>-/-</sup> Kupffer cells were subjected to immunoblot analyses using anti-CASP1 antibody and anti-PRO-CASP1 antibody. (D) ELISAs were performed to detect serum concentrations of IL1B and IL18 from *Axl*<sup>+/+</sup> or *Axl*<sup>-/-</sup> mice (*Axl*<sup>+/+</sup> or *Axl*<sup>-/-</sup>). (E) Hematoxylin and eosin (H&E) staining of liver sections (upper left) and liver injury scores (upper right) from *Axl*<sup>+/+</sup> or *Axl*<sup>-/-</sup> mice are shown in the upper panel. Immunohistochemistry of liver sections with anti-fibrin(ogen) antibody (lower left) and fibrin(ogen) deposition area (lower right) from *Axl*<sup>+/+</sup> or *Axl*<sup>-/-</sup> mice are shown in the lower panel. Fibrin(ogen) deposition area = stained area/total image area. Scale bar: 100  $\mu$ m. (F) Immunohistochemistry of liver sections with anti-ACTA2 antibody, anti-ADGRE1/F4/80 antibody (ADGRE1), anti-MAP1LC3B antibody (MAP1LC3B) and anti-ATG5 antibody (ATG5) from *Axl*<sup>+/+</sup> or *Axl*<sup>-/-</sup> mice. Each staining area = stained area/total image area. DAPI staining was performed to visualize nuclei. Scale bar: 100  $\mu$ m. "–", vehicle treatment; "+", CCl<sub>4</sub> treatment. All data represent the mean  $\pm$  SEM from 3 independent experiments. \**P* < 0.05; \*\**P* < 0.01.

We also provide molecular evidence showing that the cytoplasmic domain of AXL is critical for autophagy induction. Our experiments with several AXL mutants revealed that 2 autophosphorylated tyrosine residues (Tyr815 and Tyr860) in

the cytoplasmic domain of AXL are required for autophagy induction. Our next question addressed which downstream signaling molecule mediates autophagy induction through GAS6-AXL signaling. GAS6-AXL signaling has been linked to

multiple downstream pathways through GRB2 and PtdIns3K.<sup>38</sup> Previously identified downstream effector molecules of GRB2 and PtdIns3K that transmit GAS6-AXL signaling include MAPK14, MAP2K1/2, MAPK1/3, and MAPK8/9/10, which promote cell migration, proliferation, and survival of different cell types.<sup>38</sup> GAS6-AXL signaling also mediates activation of NFκB through PtdIns3K.<sup>38,39</sup> We found that treatment with the MAPK11/14 inhibitor alone was sufficient to block GAS6-AXL signaling-mediated autophagy induction. This observation was further confirmed by the result that inhibition of MAPK14 activity mediated through shRNA abolished GAS6-AXL signaling-mediated autophagy induction.

The NLRP3 inflammasome in macrophages is a protein complex which consists of NLRP3, PYCARD, and CASP1.<sup>40,41</sup> After recognition of several pathogen-associated molecular patterns, NLRP3 inflammasomes control the maturation and secretion of IL1B and IL18 by activating CASP1.<sup>40,41</sup> *Nlrp3*, *Pycard* or *Casp1* deficient mice show significant defects in secretion of IL1B and IL18 after treatment with LPS and ATP.<sup>26,27</sup> Recently, an inverse relationship between autophagy induction and NLRP3 inflammasome activation has been proposed.<sup>16-18</sup> Indeed, mice lacking genes encoding several autophagy proteins such as ATG16L1, BECN1, and MAP1LC3B produce excessive amounts of IL1B and IL18 in response to LPS or LPS and ATP.<sup>16-18</sup>

To clarify the biological relationship between autophagy induction through GAS6-AXL signaling and NLRP3 inflammasome activation, we explored the possibility that autophagy induction through GAS6-AXL signaling may inhibit NLRP3 inflammasome activation in macrophages. Our results clearly indicated that autophagy induction through GAS6-AXL signaling inhibits NLRP3 inflammasome-dependent activation of CASP1. Previous observations show that autophagy inhibits NLRP3 inflammasome activation by reducing the concentration of reactive oxygen species (ROS).<sup>17,18</sup> Supporting this idea, several observations show that autophagy negatively regulates ROS generation,<sup>16,42</sup> and NLRP3 inflammasome activity is suppressed by ROS blockade.<sup>41</sup> In agreement with these reports, we detected less ROS in GAS6-treated *Axl*<sup>+/+</sup> macrophages than in untreated *Axl*<sup>+/+</sup> macrophages during NLRP3 inflammasome activation (Fig. S19A). Also, PYCARD multimer formation was decreased in *Axl*<sup>+/+</sup> macrophages treated with GAS6, but not in *axl*<sup>-/-</sup> macrophages (Fig. S19B). Nevertheless, most previous observations have used specific gene-deficient mouse models to speculate on the relationship between autophagy and NLRP3 inflammasome activation.<sup>16-18</sup> However, our results provide direct evidence showing that autophagy formation by GAS6-AXL signaling indeed inhibits NLRP3 inflammasome activity.

Previously, 2 independent studies have shown that GAS6-AXL signaling inhibits the secretion of proinflammatory cytokines. The first study demonstrates that GAS6-AXL signaling induces the expression of *Twist1* (twist family bHLH transcription factor 1), which inhibits the NFκB dependent transcription of *Tnf*.<sup>7</sup> The second study indicates that IFNA receptor-STAT1-dependent AXL signaling induces *Socs1* and *Socs3*, which inhibit toll-like receptor and cytokine receptor signaling.<sup>8</sup> Our results showed that autophagy induced by GAS6-AXL signaling is NFκB-independent and that mRNA levels of *Il1b* and *Il18* do

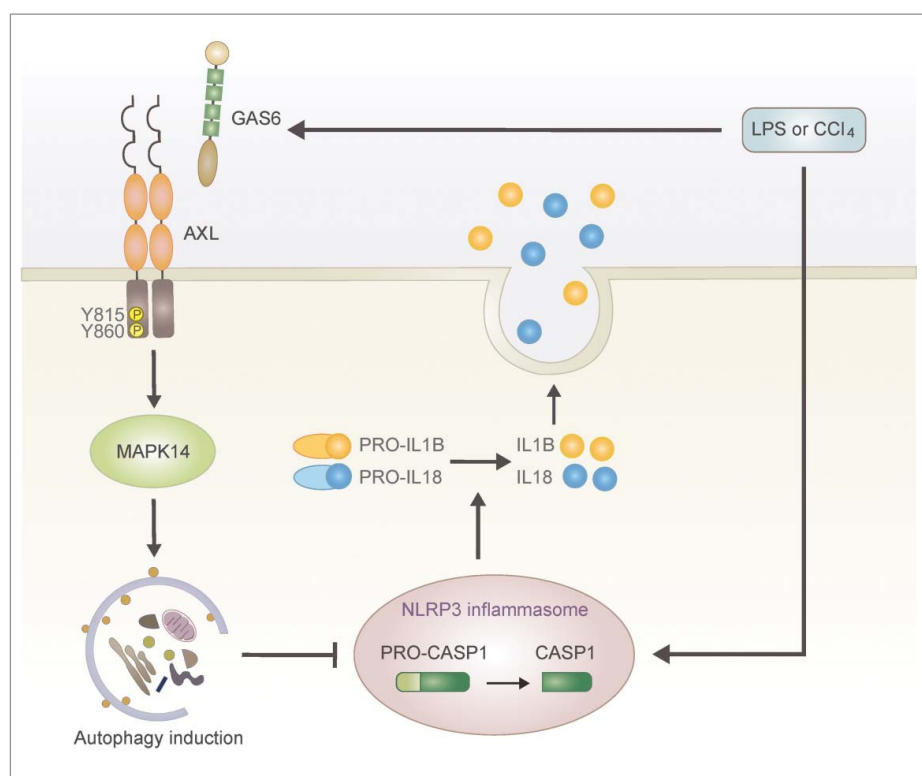
not change after treatment with GAS6. Also, we showed that the inhibition of NLRP3 inflammasome activation via GAS6-AXL signaling is independent of IFNA-STAT1 signaling. Therefore, the proposed mechanism herein by which GAS6-AXL signaling inhibits proinflammatory cytokine secretion is different from those proposed in the other studies mentioned above.<sup>7,8</sup> Our results demonstrate a novel mechanism of GAS6-AXL signaling which blocks proinflammatory cytokine production by inhibiting NLRP3 inflammasome mediated CASP1 activation through autophagy induction. Therefore, 2 previous observations together with our results, strongly suggest that GAS6-AXL signaling is important in regulation of the inflammatory response using different effector molecules such as TWIST1, SOCS1, SOCS3 or MAPK14.<sup>7,8</sup>

Increasing evidence demonstrates the importance of NLRP3 inflammasome regulation in Kupffer cells during liver inflammation. For example, NLRP3 inflammasome activation in Kupffer cells often causes severe liver inflammation.<sup>31,32</sup> Also, a recent study reports spontaneous generation of severe liver inflammation in myeloid cell-specific hyperactive *Nlrp3* transgenic mice.<sup>43</sup> In the current study, we demonstrated the physiological relevance of GAS6-AXL signaling-mediated autophagy induction on NLRP3 inflammasome-mediated CASP1 activation in LPS- or CCl<sub>4</sub>-induced acute liver injury models. First, we demonstrated that GAS6 secretion and NLRP3 inflammasome activation in Kupffer cells are induced by LPS or CCl<sub>4</sub> treatment in mice. Second, we showed that autophagy induction and NLRP3 inflammasome-mediated CASP1 activation are inversely correlated. Third, *axl*<sup>-/-</sup> mice were more susceptible to LPS- or CCl<sub>4</sub>-induced acute liver injury and showed enhanced expression of IL1B and IL18. The combined results suggest that deficits in GAS6-AXL signaling in *axl*<sup>-/-</sup> Kupffer cells result in insufficient inhibition of NLRP3 inflammasome activation and thus lead to more severe liver inflammation.

Based on our results, we propose a novel role for GAS6-AXL signaling during acute liver injury. During the early stages of liver injury induced by LPS or CCl<sub>4</sub> treatment, CASP1 is activated through the NLRP3 inflammasome in Kupffer cells and proinflammatory cytokines such as IL1B and IL18 are promptly secreted by kupffer cells (Fig. 7). At the same time GAS6 levels are substantially increased and the interaction between GAS6 and AXL leads to autophagy induction in Kupffer cells (Fig. 7). Then, the autophagy prevents further activation of CASP1 through inhibition of NLRP3 inflammasome activation in kupffer cells (Fig. 7).

Although the effect of GAS6-AXL signaling in the liver seems to be antiinflammatory in conditions of acute inflammation, 2 previous observations have found that TAM signaling promotes liver fibrosis during chronic inflammation. The first study demonstrates that *Gas6* deficiency attenuates hepatic steatosis by reducing macrophage infiltration and attenuating hepatic progenitor cell activation.<sup>44</sup> The second study indicates that GAS6-AXL signaling promotes liver fibrogenesis by hepatic stellate cell activation.<sup>45</sup> These results, along with ours, may reflect differential effects of TAM signaling that are dependent on particular downstream molecules in different target cells since multiple and divergent downstream effectors are involved in GAS6-AXL signaling.<sup>38</sup>





**Figure 7.** Schematic summary for the role of GAS6-AXL signaling-mediated autophagy during LPS- or CCl<sub>4</sub>-mediated acute liver injury. Our results suggest that autophagy induced by GAS6-AXL signaling represses hepatic inflammatory response via a negative feedback loop. During the early stages of liver inflammation induced by LPS or CCl<sub>4</sub>, Kupffer cells promptly secrete mature IL1B and IL18 through NLRP3 inflammasome-mediated activation of CASP1. Simultaneously, GAS6 induced by LPS or CCl<sub>4</sub> binds to AXL, which subsequently leads to the induction of autophagy. Then, autophagy inhibits further secretion of mature IL1B and IL18 by blocking NLRP3 inflammasome activation.

In conclusion, this study shows that the GAS6-AXL signaling pathway mediates autophagy induction in macrophages through MAPK14, and that this effect depends on the Tyr815 and Tyr860 residues in the cytoplasmic domain of AXL. Furthermore, we show that GAS6-AXL signaling-mediated autophagy induction in Kupffer cells prevents more severe inflammation by inhibiting NLRP3 inflammasome activation in murine acute liver injury models induced by LPS or CCl<sub>4</sub>. These findings provide the first evidence that AXL signaling regulates autophagy in macrophages, and that autophagic activity in Kupffer cells is a key factor that determines the extent of secretion of proinflammatory cytokines such as IL1B and IL18 during acute liver injury.

## Materials and methods

### Antibodies and reagents

The antibodies used are the following: anti-MAP1LC3B antibody (Cell Signaling Technology, 2775), anti-MAPK11 antibody (Cell Signaling Technology, 2339), anti-MAPK14 antibody (Cell Signaling Technology, 9218), anti-phosphorylated MAPK antibody (Cell Signaling Technology, 9216), anti-ATG5 antibody (Cell Signaling Technology, 8540), anti-phosphorylated STAT1 antibody (Cell Signaling Technology, 9167), anti-ACTB/actin,  $\beta$  antibody (Sigma, A5441) and anti-ACTA2 antibody (mouse IgG<sub>2a</sub>; Sigma, A2547), anti-mouse AXL antibody (rat IgG<sub>2a</sub>; R&D systems, MAB8541), rat IgG<sub>2a</sub> isotype control (R&D systems, MAB006), anti-mouse MERTK antibody (rat IgG<sub>1</sub>; R&D

systems, MAB591), rat IgG<sub>1</sub> isotype control (R&D systems, MAB005), biotinylated anti-mouse TYRO3 antibody (rat IgG<sub>1</sub>; R&D systems, BAM759), rat IgG<sub>1</sub> biotinylated isotype control (R&D systems, IC005B), anti-mouse AXL neutralizing antibody (goat polyclonal; R&D systems, AF854), anti-mouse MERTK neutralizing antibody (goat polyclonal; R&D systems, AF591), anti-mouse TYRO3 neutralizing antibody (goat polyclonal; R&D systems, AF759), goat IgG antibody isotype control (R&D systems, AB-108-C), FITC-conjugated anti-ITGAM/CD11b antibody (rat IgG<sub>2b</sub>; eBioscience, 11-0112), FITC-conjugated rat IgG<sub>2b</sub> isotype control (eBioscience, 11-4031), anti-mouse AXL antibody (Santa Cruz Biotechnology, sc-20741), anti-IL18 antibody (Santa Cruz Biotechnology, sc-7954), anti-RELA antibody (Santa Cruz Biotechnology, sc-372), anti-STAT1 antibody (Santa Cruz Biotechnology, sc-346), anti-CASP1 antibody (Santa Cruz Biotechnology, sc-514), anti-PYCARD antibody (Santa Cruz Biotechnology, sc-22514-R), goat anti-mouse IgG-HRP (Santa Cruz Biotechnology, sc-2005), goat anti-rabbit IgG-HRP (Santa Cruz Biotechnology, sc-2004), anti-ADGRE1/F4/80 antibody (rat IgG<sub>2a</sub>; Thermo Fisher Scientific, MF48000), Alexa Fluor 488-conjugated anti-mouse IgG (Thermo Fisher Scientific, A-11001), Alexa Fluor 488-conjugated anti-rat IgG (Thermo Fisher Scientific, A-11006), Alexa Fluor 594-conjugated anti-rabbit IgG (Thermo Fisher Scientific, A-11037), PE-conjugated anti-ADGRE1/F4/80 antibody (Thermo Fisher Scientific, MF48004), rabbit anti-mouse fibrin(ogen) antiserum (Molecular Innovations, ASMFBN), anti-IL1B antibody (BioVision, 5129-100), anti-mouse IFNA receptor antibody (mouse IgG<sub>1</sub>; BioXcell, BE0241), mouse IgG<sub>1</sub> isotype control (BioXcell, BE0083),



biotinylated goat anti-rat IgG (Vector Laboratories, BA-9400), Streptavidin-PE (BD Biosciences, 349023), and anti-PE microbeads (Miltenyi Biotec, 130-048-801). The reagents used are the following: Recombinant mouse GAS6 (R&D systems, 986-GS), R428 (AXL inhibitor; Selleck Chemicals, S2841), SP600125 (MAPK8/9/10 inhibitor; Sigma, S5567), glibenclamide (NLRP3 inflammasome inhibitor; Sigma, G0639), U0126 (MAP2K1/2 and MAPK1/3 inhibitor; InvivoGen, tlr-u0126), SB203580 (MAPK11/14 inhibitor; InvivoGen, tlr-sb20), BKM120 (PtdIns3K inhibitor; Selleck Chemicals, S2247), rapamycin (LC Laboratories, R5000), LPS (Sigma, L4391), CQ (Sigma, C6628), ATP (Sigma, A2383), CCl<sub>4</sub> (Junsei Chemical, 33650-0330), Mito-SOX Red mitochondrial superoxide indicator (Invitrogen, M36008).

### Cells

Murine macrophage cell lines (P388D1 and J774) were maintained in DMEM (Invitrogen, 11965-084) supplemented with 5% fetal bovine serum (Hyclone, SH30071) and 1% penicillin/streptomycin (Invitrogen, 15140-122). The pBABE-puro mCherry-EGFP-LC3B plasmid (Addgene, 22418; deposited by Dr. Jay Debnath). mCherry-EGFP-MAP1LC3B-expressing P388D1 and J774 cell lines were established as previously described.<sup>46</sup>

Peritoneal macrophages were isolated from *axl*<sup>-/-</sup>, *Axl*<sup>+/+</sup>, *Atg7*<sup>fl/fl</sup> *Lyz2*-Cre<sup>+</sup> (*Atg7*<sup>fl/fl</sup> CKO) or *Atg7*<sup>fl/fl</sup> *Lyz2*-Cre<sup>-</sup> (*Atg7*<sup>fl/fl</sup> CTRL) mice (8-wk old) as previously described.<sup>47</sup> Briefly, mice were intraperitoneally injected with 1 ml of 3% Brewer thioglycollate (BD Biosciences, 211716). Three d after injection, cells were isolated by flushing out the peritoneal cavity using 10 ml of phosphate-buffered saline (PBS; 135 mM NaCl, 2.7 mM KCl, 10 mM Na<sub>2</sub>HPO<sub>4</sub>, 2 mM KH<sub>2</sub>PO<sub>4</sub>, pH 7.4) without calcium and magnesium. Cells were then plated on culture dishes and incubated at 37°C and 5% CO<sub>2</sub> in DMEM/F-12 medium (Invitrogen, 11330-032) supplemented with 10% (v/v) fetal bovine serum and 1% penicillin/streptomycin for 4 h. Subsequently, nonadherent cells were removed by gently washing 3 times with warm PBS. Adherent cells were counted, stained with FITC-conjugated anti-ITGAM/CD11b antibody, and analyzed using flow cytometry. More than 90% of cells were ITGAM-positive.

### Measurement of autophagy induction

Cells were treated with various concentrations of recombinant GAS6, CQ and/or serum deprivation for 24 h. Also, various combinations of neutralizing antibodies including anti-mouse AXL antibody (2 µg/ml), anti-mouse MERTK antibody (2 µg/ml), and anti-mouse TYRO3 antibody (2 µg/ml), or inhibitors including R428 (AXL inhibitor, 2.5 µM), SP600125 (MAPK8/9/10 inhibitor, 10 µM), U0126 (MAP2K1/2 and MAPK1/3 inhibitor, 5 µM), SB203580 (MAPK11/14 inhibitor, 2.5 µM), BKM120 (PtdIns3K inhibitor, 1 µM) and rapamycin (MTOR inhibitor, 100 nM) were added to block autophagy induction after GAS6 treatment. After treatment, autophagy induction in each cell was measured via immunoblotting and confocal microscopy. Also, *Atg5*, *Becn1* and *Map1lc3b* mRNA levels

were measured by quantitative reverse-transcriptase polymerase chain reaction (qRT-PCR).

### Western blot analyses

Cells were washed 3 times with PBS, centrifuged, and lysed with RIPA lysis solution (50 mM Tris, pH 7.4, 150 mM NaCl, 1% NP-40 [Sigma, 74385], 0.5% sodium deoxycholate [Sigma, D6750], 0.1% SDS [Sigma, L4509]) containing 200 µg/ml of phenylmethylsulfonyl fluoride (Sigma, P7626), phosphatase inhibitor cocktail (Sigma, P0044) and protease inhibitor cocktail (Millipore, 535140). The cell lysates were subsequently resolved by 12% SDS-polyacrylamide gel electrophoresis, transferred onto Immobilon P membranes (Millipore, IPVH00010), and immunoblotted with appropriate antibodies. Immunoreactive bands were visualized using an ECL solution (GE Healthcare, RPN2232). To determine the MAP1LC3B-I to MAP1LC3B-II ratio, immunoreactive bands were quantified using ImageJ software version 1.43u (National Institutes of Health, Bethesda, MD, USA). Then, the values of MAP1LC3B-I to MAP1LC3B-II ratio were relative to the control value of the experiment. To quantify the relative expression of other proteins, immunoreactive bands were normalized to ACTB levels.

### Confocal microscopy

To observe autophagy induction, mCherry-EGFP-MAP1LC3B-expressing P388D1 cells and J774 cells were treated with various combinations of recombinant GAS6, neutralizing antibody and/or inhibitors. The cells were then washed 3 times with PBS and fixed with 4% paraformaldehyde (Sigma, P6148) in PBS at room temperature for 10 min. After washing 3 times with PBS, cells were stained with a mounting solution containing DAPI (Vector Laboratories, H-1200) and imaged by confocal microscopy on an LSM 5 EXCITER (Carl-Zeiss, Oberkochen, Germany).

### qRT-PCR

The mRNA transcripts of mouse *Atg5*, *Becn1*, *Map1lc3b*, *Gas6*, *Il1b*, *Il18*, *Nlrp3*, *Pyard* and *Casp1* were quantitatively measured by real-time PCR analyses. The mRNA transcript of mouse *Gapdh* was used as an internal control for qRT-PCR. Briefly, total RNAs from cells or tissues were isolated using Trizol reagent according to the manufacturer's protocol (Thermo Fisher Scientific, 15596-026), and reverse transcribed into cDNA using the First-Strand cDNA Synthesis Kit with oligo-dT primers and Super-Script RT (Thermo Fisher Scientific, K1622). After cDNA synthesis, quantitative real-time PCR was conducted using a 7500 Real-time PCR system (Applied Biosystems, Foster City, CA, USA). The primer pairs used for qRT-PCR are listed in Table S1.

### Cloning and expression of mutant *Axl*

Several amino acid substitution mutants of *Axl* were cloned with PCR from the mouse *Axl* gene (GenBank accession BC050914) and expressed in macrophages (J774 cell) via

retroviral transduction. The cDNA of wild-type mouse *Axl* was isolated by RT-PCR using total RNAs of P388D1 as a template. The expression vectors encoding wild-type mouse *Axl* (WT *Axl*), the cytoplasmic domain deletion mutant of *Axl* (*Axl*<sup>CYΔ</sup>), *Axl* mutants with a single amino acid substitution (*Axl*<sup>Y696F</sup>, *Axl*<sup>Y697F</sup>, *Axl*<sup>Y773F</sup>, *Axl*<sup>Y815F</sup>, and *Axl*<sup>Y860F</sup>), and an *Axl* mutant with a double amino acid substitution (*Axl*<sup>Y815F,Y860F</sup>) were constructed by cloning PCR products using *NotI* and *SalI* restriction sites in the retroviral vector pLNCX2 (Clontech, 631503). PCR was performed using the cDNA of wild-type mouse *Axl* as a template. The primer pairs used for each expression vector are listed in Table S2. The schematic diagrams of individual proteins expressed from DNA constructs are shown in Supporting Fig. 5A. Each DNA construct was then transfected into 293GPG cells using Lipofectamine (Thermo Fisher Scientific, 11668-019). After 3 d, the supernatant from each transfectant was used to infect J774 cells using 1 μg/ml of polybrene (Sigma, H9268). To establish stable cell lines, each group of infected cells was selected with 1.5 mg/ml neomycin (Sigma, N1876). Proper cell surface expression of wild-type AXL and its mutants were observed by flow cytometry analyses.

### Flow cytometry analyses

Flow cytometry analyses were performed to determine the cell surface expression of mouse AXL, MERTK, TYRO3 and ITGAM. For surface staining of AXL or MERTK, cells were stained with either purified anti-AXL antibody (rat IgG<sub>2a</sub>) or anti-MERTK antibody (rat IgG<sub>1</sub>), followed by biotinylated goat anti-rat IgG and streptavidin-PE. Rat IgG<sub>2a</sub> and rat IgG<sub>1</sub> control were used as isotype controls. For surface staining of TYRO3, cells were stained with biotinylated anti-mouse TYRO3 antibody (rat IgG<sub>1</sub>) in combination with streptavidin-PE. Biotinylated rat IgG<sub>1</sub> was used as an isotype control. To visualize ITGAM surface expression, cells were stained with FITC-conjugated anti-ITGAM antibody (rat IgG<sub>2b</sub>). FITC-conjugated rat IgG<sub>2b</sub> control was used as an isotype control. After washing several times with PBS, all stained cells were resuspended in PBS and analyzed by flow cytometry using a FACS-Calibur with CellQuest software (BD Biosciences, San Jose, CA, USA).

### RT-PCR

The mRNA transcripts of mouse *Mapk11* and *Mapk14* were measured by RT-PCR analyses. The cDNA synthesis was described as above. After cDNA synthesis, PCR was conducted using a SimpliAmp Thermal Cycler (Thermo Fisher Scientific). The resulting PCR products were loaded onto a 1.5% agarose gel containing ethidium bromide, and were visualized using ultraviolet light. The primer pairs used for qRT-PCR are listed in Table S3.

### Co-immunoprecipitation

AXL-expressing J774 cells were washed in PBS and resuspended in cell lysis buffer (50 mM Tris HCl, pH 7.4, 150 mM NaCl, 1% NP-40) containing 200 μg/ml of phenylmethylsulfonyl fluoride,

phosphatase inhibitor cocktail and protease inhibitor cocktail. The lysates were incubated with anti-MAPK11 antibody or anti-MAPK14 antibody and precipitated with protein G sepharose<sup>TM</sup> Fast Flow (GE Healthcare, 17-0618-01). The precipitated proteins were resolved via SDS-PAGE, transferred to Immobilon-P membranes, and immunoblotted with anti-phosphorylated MAPK antibody using the ECL system. Anti-ACTB antibody was utilized as an internal control.

### Inhibition of gene expression by shRNAs

The lentiviral plasmids expressing shRNAs directed against several distinct regions of *Mapk14* (sc-29434) or *Rela* (sc-29411) were purchased from Santa Cruz Biotechnology together with control shRNA plasmids (sc-108060). Mouse *Axl*-expressing J774 cells were transfected with each shRNA-containing plasmid using Lipofectamine 2000 (Thermo Fisher Scientific, 11668-019) according to the manufacturer's instructions. After transfection, cells were selected with 4 μg/ml of puromycin (Sigma, P7255). Inhibition of MAPK14 expression and RELA expression were determined by immunoblotting with appropriate antibodies.

### Measurement of NLRP3 inflammasome activation

Murine macrophages were treated with ATP, IFNα receptor blocking antibody, LPS, glibenclamide, and/or recombinant GAS6 as indicated and the cells were tested for inflammasome activation by immunoblotting and ELISA.

### ELISAs

IL1B and IL18 secretion levels were quantified by sandwich ELISAs using mouse IL1B (eBioscience, BMS6002) and IL18 ELISA kits (eBioscience, BMS618/3) according to the manufacturer's instructions.

### Animal studies

*Axl* deficient (*axl*<sup>-/-</sup>) mice were kindly provided by Dr. Lemke (Salk Institute, La Jolla, CA) and backcrossed into the C57BL/6J strain for more than 9 generations. *Atg7*-floxed mice (*Atg7*<sup>fl/fl</sup>, C57BL/6 background) were kindly provided by Dr. Komatsu (Tokyo Metropolitan Institute of Medical Science, Tokyo, Japan). *Atg7*<sup>fl/fl</sup> mice were crossed with B6.129P2-*Ly2*<sup>tm1(cre)lfo</sup>/J mice (Jackson Laboratory, 004781) where Cre recombinase expression is under the control of lysozyme M promoter to generate *Atg7* conditional knockout mice with myeloid lineage cell-specific deletion of *Atg7* (*Atg7*<sup>fl/fl</sup> CKO) and their wild-type counterparts (*Atg7*<sup>fl/fl</sup> CTRL). More information about the generation of *Atg7*<sup>fl/fl</sup> CKO and *Atg7*<sup>fl/fl</sup> CTRL mice was previously described.<sup>28,29</sup> Animal models of acute liver injury were created by injecting either LPS or CCl<sub>4</sub> into mice.<sup>48,49</sup> To induce LPS-challenged acute liver injury, mice were intraperitoneally injected with 2.5 μg/g of PBS-dissolved LPS. Mice were sacrificed at 3, 6, and 12 h after LPS injection and mRNA transcripts of *Gas6* from liver or spleen tissue of sacrificed mice were monitored by qRT-PCR. In addition, Kupffer cells, sera, and several tissues were harvested from mice sacrificed at 12 h after LPS

injection to perform qRT-PCR analyses, western blot analyses, histological analyses, immunohistochemistry, and to measure serum GPT, GOT1, and cytokine secretions. For induction of CCl<sub>4</sub>-mediated acute liver injury, mice were injected intraperitoneally with 2  $\mu$ l/g of CCl<sub>4</sub> mixed with corn oil at a ratio of 1:9. Mice were sacrificed at 1, 2, and 3 d after CCl<sub>4</sub> injection, mRNA transcripts of *Gas6* from liver tissue of sacrificed mice were monitored by qRT-PCR. Also, Kupffer cells, sera, and liver were harvested from mice sacrificed at 1, 2, and 3 d after CCl<sub>4</sub> injection to perform qRT-PCR analyses, western blot analyses, histological analyses, immunohistochemistry, and to measure serum GPT, GOT1, and cytokine secretions. To evaluate the effect of glibenclamide in acute liver injury model, mice were injected with LPS and 1  $\mu$ g/g of DMSO-dissolved glibenclamide or CCl<sub>4</sub> and glibenclamide. Kupffer cells and sera from mice were harvested to perform western blot analyses and to measure cytokine secretions. All animals received proper care in accordance with a protocol based on the National Institutes of Health Guide for the Care and Use of Laboratory Animals and approved by the Institutional Animal Care and Use Committee at Korea University and Chungnam National University (protocol numbers: KUIACUC-2014-259 and CNUH-014-A0007).

### Histological analyses and immunochemistry

Tissues were fixed with 10% neutral buffered formalin (Sigma, HT5011) and embedded in paraffin. Sections measuring 5  $\mu$ m were cut using a Leica CM1800 cryostat (Leica Microsystems, Wetzlar, Germany), air dried at room temperature, and stained with hematoxylin and eosin (H&E). The severity of liver injury and necroinflammatory activity were scored using H&E stained sections according to standard methods as previously described.<sup>50,51</sup> The severity of liver injury observed in the tissue sections was scored as follows: 0, minimal or no evidence of injury; 1, mild injury consisting of cytoplasmic vacuolation and focal nuclear pyknosis; 2, moderate to severe injury with extensive nuclear pyknosis, cytoplasmic hypereosinophilia, and loss of intercellular borders; and 3, severe necrosis with disintegration of the hepatic cords, hemorrhage, and neutrophil infiltration. Ten different areas ( $\times$  100 fields) were examined for necroinflammatory activity. The necroinflammatory activity observed in the tissue sections was scored as follows: 0, no affected area; 1, less than 2 areas; 2, between 2 and 4 areas; 3, between 5 and 10 areas; 4, more than 10 areas with necroinflammatory activity.

For detection of fibrin deposition, livers were perfused through a portal vein with PBS and liver specimens were rapidly sampled, fixed in 10% zinc fixative (BD Biosciences, 550523), and embedded in paraffin. Tissue sections were incubated overnight with rabbit anti-mouse fibrinogen antiserum (1:5,000) followed by treatment with the rabbit Vectastain Elite ABC kit (Vector Laboratories, PK-6100). Antigen-antibody complexes were detected using a DAB Substrate Kit (Vector Laboratories, SK-4100). Immunohistochemical analysis was performed with an anti-ACTA2 antibody coupled with Alexa Fluor 488-conjugated anti-mouse IgG (green fluorescence), an anti-ADGRE1/F4/80 antibody coupled with Alexa Fluor 488-conjugated anti-rat IgG (green fluorescence), an anti-MAP1LC3B antibody

coupled with Alexa Fluor 594-conjugated anti-rabbit IgG (red fluorescence) and an anti-ATG5 antibody coupled with Alexa Fluor 594-conjugated anti-rabbit IgG (red fluorescence) using a Bond Max autostainer according to the manufacturer's protocol (Leica Microsystems, Wetzlar, Germany).

### Kupffer cell isolation

Kupffer cells were isolated from mice as described previously.<sup>32</sup> Briefly, the portal vein of anesthetized mice was cannulated, and the liver was perfused at 7 mL/min for 10 min with Gey balanced salt solution (Sigma, G9779) without Ca<sup>2+</sup> at 37°C. Subsequently, perfusion with Gey balanced salt solution containing 1.5 mM CaCl<sub>2</sub> and 0.5 mg/mL of collagenase type IV (Invitrogen, 17104019) was performed for 10 min. The digested liver was dissected out thoroughly on a petri dish and then the supernatant was filtered. The nonparenchymal cell fraction containing Kupffer cells was separated by 3 cycles of differential centrifugation (30  $\times$  g for 3 min). The supernatant was collected and centrifuged (400  $\times$  g for 3 min) to obtain nonparenchymal cell pellets. Isolated nonparenchymal cells were stained with PE-conjugated anti-ADGRE1/F4/80 antibody coupled with anti-PE microbeads and then Kupffer cells were isolated using a magnetic bead-associated cell sorting system (Miltenyi Biotec, Bergisch Gladbach, Germany). The purity of Kupffer cells was more than 90%, as assessed by flow cytometry analyses.

### Measurement of plasma GPT and GOT1

Plasma GPT and GOT1 levels were measured by the standard colorimetric method using Asan GPT and GOT1 kits (Asan Pharmaceutical, AM101-K) according to the manufacturer's instructions.

### Measurement of ROS

Measurement of mitochondrial superoxide was done using MitoSOX Red Mitochondrial Superoxide Indicator according to the manufacturer's instructions. Briefly, isolated mouse peritoneal macrophages were treated with LPS (100 ng/ml), ATP (5 mM) and/or recombinant GAS6 (100 ng/ml) for 6 h. After treatment, cells were incubated in Hank's balanced salt solution (Invitrogen, 14025-092) with 5  $\mu$ M MitoSOX Red for 10 min at 37°C and washed with PBS. Then, cells were harvested and assessed by flow cytometry.

### PYCARD pyroptosome detection

PYCARD pyroptosomes were detected as described previously.<sup>52</sup> Briefly, isolated mouse peritoneal macrophages were treated with LPS (100 ng/ml), ATP (5 mM) and/or recombinant GAS6 (100 ng/ml) for 6 h. After treatment, cells were harvested and resuspended in 0.5 ml of ice-cold buffer (20 mM HEPES-KOH, pH 7.5, 150 mM KCl, 1% NP-40, 0.1 mM PMSF and protease inhibitor cocktail), and lysed by shearing 10 times using a 21-gauge needle. Then the cell lysates were centrifuged at 6,000  $\times$  g for 10 min at 4°C, and the pellets were washed with PBS. The pellets were resuspended in 0.5 ml of 4 mM DSS in PBS and cross-linked in a shaking incubator for 30 min at

37°C, and then centrifuged at  $6,000 \times g$  for 10 min. The cross-linked pellets were resuspended in 30  $\mu$ l SDS sample buffer, separated by 12% SDS-polyacrylamide gel electrophoresis and immunoblotted with anti-mouse PYCARD antibody.

### Statistical analyses

Mean values were compared using a Student *t* test for independent variables. Significant differences as determined by *P* values of less than 0.05 and 0.01 are indicated with asterisks (\*) and (\*\*), respectively, on each graph.

### Abbreviations

|                       |   |
|-----------------------|---|
| ACTA2                 | actin, $\alpha$ 2, smooth muscle, aorta   |
| ACTB                  | actin, $\beta$  |
| ADGRE1                | adhesion G protein-coupled receptor E1  |
| ATG5                  | autophagy-related 5   |
| ATG7                  | autophagy-related 7   |
| AXL                   | AXL receptor tyrosine kinase  |
| AXL <sup>CYΔ</sup>    | deletion mutant lacking the cytoplasmic domain of AXL                           |
| BECN1                 | beclin 1, autophagy related   |
| CASP1                 | caspase 1   |
| CCl <sub>4</sub>      | carbon tetrachloride  |
| CQ                    | chloroquine   |
| GAS6                  | growth arrest specific 6  |
| GOT1                  | glutamic-oxaloacetic transaminase 1, soluble                                    |
| GPT                   | glutamic pyruvic transaminase, soluble  |
| HSC                   | hepatic stellate cell   |
| IFN                   | interferon  |
| IFNAR1                | interferon $\alpha$ and $\beta$ receptor subunit 1                              |
| IL1B                  | interleukin 1, $\beta$  |
| IL18                  | interleukin 18  |
| ITGAM                 | integrin $\alpha$ M   |
| LPS                   | lipopolysaccharide  |
| MAP1LC3B              | microtubule-associated protein 1 light chain 3 $\beta$                          |
| MAPK                  | mitogen-activated protein kinase  |
| MAP2K1/2              | mitogen-activated protein kinase kinase 1/2                                     |
| mCherry-EGFP-MAP1LC3B | tandem fusion of MAP1LC3B protein to acid-insensitive mCherry together with GFP |
| MERTK                 | c-mer proto-oncogene tyrosine kinase  |
| MTOR                  | mechanistic target of rapamycin   |
| NFKB                  | nuclear factor of kappa light polypeptide gene enhancer in B-cells              |
| NLRP3                 | NLR family, pyrin domain containing 3   |
| PtdIns3K              | class III phosphatidylinositol 3-kinase   |
| PYCARD                | PYD and CARD domain containing  |

qRT-PCR

RELA

RTK

SMA

ROS

STAT1

TAM

TWIST1

TYRO3

WT AXL

quantitative reverse-transcriptase polymerase chain reaction  
v-rel avian reticuloendotheliosis viral oncogene homolog A  
receptor tyrosine kinases  
smooth muscle actin  
reactive oxygen species  
signal transducer and activator of transcription 1  
TYRO3, AXL and MERTK family of RTKs  
twist family bHLH transcription factor 1  
TYRO3 protein tyrosine kinase 3  
wild-type AXL

### Disclosure of potential conflicts of interest

No potential conflicts of interest were disclosed.

### Acknowledgments

We are very grateful to Dr. Lemke (Salk Institute, La Jolla, CA) for providing *Axl* deficient (*axl*<sup>-/-</sup>) mice, Dr. Komatsu (Tokyo Metropolitan Institute of Medical Science, Tokyo, Japan) for providing *Atg7*-floxed mice (*Atg7*<sup>fl/fl</sup>) and Dr. Debnath (University of California San Francisco, San Francisco, CA) for providing a cDNA construct encoding mCherry-EGFP-MAP1LC3B (Addgene, 22418).

### Funding

This work was supported by a grant from the Next-Generation Bio-Green 21 program (project no. PJ01113001), Rural Development Administration, Republic of Korea. We would also like to thank School of Life Sciences and Biotechnology for BK21 PLUS, Korea University for supporting the publication fee.

### ORCID

Jihye Han  <http://orcid.org/0000-0002-9477-0270>  
Joonbeom Bae  <http://orcid.org/0000-0002-2502-9147>  
Chang-Yong Choi  <http://orcid.org/0000-0003-2139-3109>  
Sang-Pil Choi  <http://orcid.org/0000-0001-8797-8332>  
Hyung-Sik Kang  <http://orcid.org/0000-0002-2295-9293>  
Eun-Kyeong Jo  <http://orcid.org/0000-0002-9623-9037>  
Jongsun Park  <http://orcid.org/0000-0002-4690-1854>  
Young Sik Lee  <http://orcid.org/0000-0002-6709-3809>  
Hyun-Seuk Moon  <http://orcid.org/0000-0002-5216-2090>  
Chung-Gyu Park  <http://orcid.org/0000-0003-4083-8791>  
Myung-Shik Lee  <http://orcid.org/0000-0003-3292-1720>  
Taehoon Chun  <http://orcid.org/0000-0002-5940-8620>

### References

- [1] Rockey DC, Bell PD, Hill JA. Fibrosis- a common pathway to organ injury and failure. *N Engl J Med* 2015; 372:1138-49; PMID:25785971; <http://dx.doi.org/10.1056/NEJMr1300575>
- [2] Seki E, Schwabe RF. Hepatic inflammation and Fibrosis: Functional links and key pathways. *Hepatology* 2015; 61:1066-79; PMID:25066777; <http://dx.doi.org/10.1002/hep.27332>
- [3] Crispe IN. The liver as a lymphoid organ. *Annu Rev Immunol* 2009; 27:147-63; PMID:19302037; <http://dx.doi.org/10.1146/annurev.immunol.021908.132629>



- [4] Sica A, Mantovani A. Macrophage plasticity and polarization: in vivo veritas. *J Clin Invest* 2012; 22:787-95; <http://dx.doi.org/10.1172/JCI59643>
- [5] Scott RS, McMahon EJ, Pop SM, Reap EA, Caricchio R, Cohen PL, Earp HS, Matsushima GK. Phagocytosis and clearance of apoptotic cells is mediated by MER. *Nature* 2001; 411:207-11; PMID:11346799; <http://dx.doi.org/10.1038/35075603>
- [6] Zagórska A, Través PG, Lew ED, Dransfield I, Lemke G. Diversification of TAM receptor tyrosine kinase function. *Nat Immunol* 2014; 15:920-8; <http://dx.doi.org/10.1038/ni.2986>
- [7] Sharif MN, Sosic D, Rothlin CV, Kelly E, Lemke G, Olson EN, Ivashkiv LB. Twist mediates suppression of inflammation by type I IFNs and Axl. *J Exp Med* 2006; 203:1891-901; PMID:16831897; <http://dx.doi.org/10.1084/jem.20051725>
- [8] Rothlin CV, Ghosh S, Zuniga EI, Oldstone MB, Lemke G. TAM receptors are pleiotropic inhibitors of the innate immune response. *Cell* 2007; 131:1124-36; PMID:18083102; <http://dx.doi.org/10.1016/j.cell.2007.10.034>
- [9] Lu Q, Lemke G. Homeostatic regulation of the immune system by receptor tyrosine kinases of the Tyro 3 family. *Science* 2001; 293:306-11; PMID:11452127; <http://dx.doi.org/10.1126/science.1061663>
- [10] Cohen PL, Caricchio R, Abraham V, Camenisch TD, Jennette JC, Roubey RA, Earp HS, Matsushima G, Reap EA. Delayed apoptotic cell clearance and lupus-like autoimmunity in mice lacking the c-mem membrane tyrosine kinase. *J Exp Med* 2002; 196:135-40; PMID:12093878; <http://dx.doi.org/10.1084/jem.20012094>
- [11] Llacuna L, Bárcena C, Bellido-Martín L, Fernández L, Stefanovic M, Mari M, García-Ruiz C, Fernández-Checa JC, García de Frutos P, Morales A. Growth arrest-specific protein 6 is hepatoprotective against murine ischemia/reperfusion injury. *Hepatology* 2010; 52:1371-9; PMID:20730776; <http://dx.doi.org/10.1002/hep.23833>
- [12] Lafdil F, Chobert MN, Deveaux V, Zafrani ES, Mavie P, Nakano T, Laperche T, Brouillet A. Growth arrest-specific protein 6 deficiency impairs liver tissue repair after acute toxic hepatitis in mice. *J Hepatol* 2009; 51:55-66; PMID:19443073; <http://dx.doi.org/10.1016/j.jhep.2009.02.030>
- [13] Klionsky DJ, Emr SD. Autophagy as a regulated pathway of cellular degradation. *Science* 2000; 290:1717-21; PMID:10634780
- [14] Levine B, Deretic V. Unveiling the roles of autophagy in innate and adaptive immunity. *Nat Rev Immunol* 2007; 7:767-77; PMID:17767194; <http://dx.doi.org/10.1038/nri2161>
- [15] Mizushima N, Levine B, Cuervo AM, Klionsky DJ. Autophagy fights disease through cellular self-digestion. *Nature* 2008; 451:1069-75; PMID:18305538; <http://dx.doi.org/10.1038/nature06639>
- [16] Saitoh T, Fujita N, Jang MH, Uematsu S, Yang BG, Satoh T, Omori H, Noda T, Yamamoto N, Komatsu M, et al. Loss of the autophagy protein Atg16L1 enhances endotoxin-induced IL-1 $\beta$  production. *Nature* 2008; 456:264-8; PMID:18849965; <http://dx.doi.org/10.1038/nature07383>
- [17] Zhou R, Yazdi AS, Menu P, Tschopp J. A role for mitochondria in NLRP3 inflammasome activation. *Nature* 2011; 469:221-5; PMID:21124315; <http://dx.doi.org/10.1038/nature09663>
- [18] Nakahira K, Haspel JA, Rathinam VA, Lee SJ, Dolinay T, Lam HC, Englert JA, Rabinovitch M, Cernadas M, Kim HP, et al. Autophagy proteins regulate innate immune responses by inhibiting the release of mitochondrial DNA mediated by the NALP3 inflammasome. *Nat Immunol* 2011; 12:222-30; PMID:21151103; <http://dx.doi.org/10.1038/ni.1980>
- [19] Beth L, Noboru M, Herbert WV. Autophagy in immunity and inflammation. *Nature* 2011; 469:323-35; PMID:21248839; <http://dx.doi.org/10.1038/nature09782>
- [20] Deretic V, Saitoh T, Akira S. Autophagy in infection, inflammation and immunity. *Nat Rev Immunol* 2013; 13:722-37; PMID:24064518; <http://dx.doi.org/10.1038/nri3532>
- [21] Klionsky DJ, Abdelmohsen K, Abe A, Abedin MJ, Abeliovich H, Acevedo Arozana A, Adachi H, Adams CM, Adams PD, Adeli K, et al. Guidelines for the use and interpretation of assays for monitoring autophagy (3rd edition). *Autophagy* 2016; 12:1-222; PMID:26799652; <http://dx.doi.org/10.1080/15548627.2015.1100356>
- [22] Mizushima N, Yoshimori T. How to interpret LC3 immunoblotting. *Autophagy* 2007; 3:542-5; PMID:17611390; <http://dx.doi.org/10.4161/auto.4600>
- [23] Mizushima N, Yoshimori T, Ohsumi Y. The role of Atg proteins in autophagosome formation. *Annu Rev Cell Dev Biol* 2011; 27:107-32; PMID:21801009; <http://dx.doi.org/10.1146/annurev-cellbio-092910-154005>
- [24] Paccez JD, Vogelsang M, Parker MI, Zerbini LF. The receptor tyrosine kinase Axl in cancer: biological functions and therapeutic implications. *Int J Cancer* 2014; 134:1024-33; PMID:23649974; <http://dx.doi.org/10.1002/ijc.28246>
- [25] Evers PA, Craxton M, Morrice N, Cohen P, Goedert M. Conversion of SB203580-insensitive MAP kinase family members to drug-sensitive forms by a single amino-acid substitution. *Chem Biol* 1998; 5:321-8; PMID:9653550; [http://dx.doi.org/10.1016/S1074-5521\(98\)90170-3](http://dx.doi.org/10.1016/S1074-5521(98)90170-3)
- [26] Li P, Allen H, Banerjee S, Franklin S, Herzog L, Johnston C, McDowell J, Paskind M, Rodman L, Salfeld J, et al. Mice deficient in IL-1  $\beta$ -converting enzyme are defective in production of mature IL-1  $\beta$  and resistant to endotoxic shock. *Cell* 1995; 80:401-11; PMID:7859282; [http://dx.doi.org/10.1016/0092-8674\(95\)90490-5](http://dx.doi.org/10.1016/0092-8674(95)90490-5)
- [27] Sutterwala FS, Ogura Y, Szczepanik M, Lara-Tejero M, Lichtenberger GS, Grant EP, Bertin J, Coyle AJ, Galán JE, Askenase PW, et al. Critical role for NALP3/CAS1/Cryopyrin in innate and adaptive immunity through its regulation of caspase-1. *Immunity* 2006; 24:317-27; PMID:16546100; <http://dx.doi.org/10.1016/j.immuni.2006.02.004>
- [28] Komatsu M, Waguri S, Ueno T, Iwata J, Murata S, Tanida I, Ezaki J, Mizushima N, Ohsumi Y, Uchiyama Y, et al. Impairment of starvation-induced and constitutive autophagy in Atg7-deficient mice. *J Cell Biol* 2005; 169:425-34; PMID:15866887; <http://dx.doi.org/10.1083/jcb.200412022>
- [29] Yang CS, Kim JJ, Lee HM, Jin HS, Lee SH, Park JH, Kim SJ, Kim JM, Han YM, Lee MS, et al. The AMPK-PPARGC1A pathway is required for antimicrobial host defense through activation of autophagy. *Autophagy* 2014; 10:785-802; PMID:24598403; <http://dx.doi.org/10.4161/auto.28072>
- [30] Guarda G, Braun M, Staehli F, Tardivel A, Mattmann C, Forster I, Farlik M, Decker T, Du Pasquier RA, Romero P, et al. Type I interferon inhibits interleukin-1 production and inflammasome activation. *Immunity* 2011; 34:213-23; PMID:21349431; <http://dx.doi.org/10.1016/j.immuni.2011.02.006>
- [31] Petrsek J, Bala S, Csak T, Lippai D, Kodys K, Menashy V, Barrieau M, Min SY, Kurt-Jones EA, Szabo G. IL-1 receptor antagonist ameliorates inflammasome-dependent alcoholic steatohepatitis in mice. *J Clin Invest* 2012; 122:3476-89; PMID:22945633; <http://dx.doi.org/10.1172/JCI60777>
- [32] Huang H, Chen HW, Evankovich J, Yan W, Rosborough BR, Nace GW, Ding Q, Loughran P, Beer-Stolz D, Billiar TR, et al. Histones activate the NLRP3 inflammasome in Kupffer cells during sterile inflammatory liver injury. *J Immunol* 2013; 191:2665-79.
- [33] Jankovic D, Ganesan J, Bscheider M, Stickel N, Weber FC, Guarda G, Follo M, Pfeifer D, Tardivel A, Ludigs K, et al. The Nlrp3 inflammasome regulates acute graft-versus-host disease. *J Exp Med* 2013; 210:1899-910; PMID:23980097; <http://dx.doi.org/10.1084/jem.20130084>
- [34] Beier JJ, Luyendyk JP, Guo L, von Montfort C, Staunton DE, Arteel GE. Fibrin accumulation plays a critical role in the sensitization to lipopolysaccharide-induced liver injury caused by ethanol in mice. *Hepatology* 2009; 49:1545-53; PMID:19291788; <http://dx.doi.org/10.1002/hep.22847>
- [35] Liu K, Zhao E, Ilyas G, Lalazar G, Lin Y, Haseeb M, Tanaka KE, Czaja MJ. Impaired macrophage autophagy increases the immune response in obese mice by promoting proinflammatory macrophage polarization. *Autophagy* 2015; 11:271-84; PMID:25650776; <http://dx.doi.org/10.1080/15548627.2015.1009787>
- [36] Dall'Armi C, Hurtado-Lorenzo A, Tian H, Morel E, Nezu A, Chan RB, Yu WH, Robinson KS, Yeku O, Small SA, et al. The phospholipase D1 pathway modulates macroautophagy. *Nat Commun* 2010; 1:142; PMID:21266992; <http://dx.doi.org/10.1038/ncomms1144>

- [37] Chikh A, Sanzà P, Raimondi C, Akinduro O, Warnes G, Chiorino G, Byrne C, Harwood CA, Bergamaschi D. iASPP is a novel autophagy inhibitor in keratinocytes. *J Cell Sci* 2014; 127:3079-93; PMID:24777476; <http://dx.doi.org/10.1242/jcs.144816>
- [38] Linger RM, Keating AK, Earp HS, Graham DK. TAM receptor tyrosine kinases: biologic functions, signaling, and potential therapeutic targeting in human cancer. *Adv Cancer Res* 2008; 100:35-83; PMID:18620092; [http://dx.doi.org/10.1016/S0065-230X\(08\)00002-X](http://dx.doi.org/10.1016/S0065-230X(08)00002-X)
- [39] Demarchi F, Verardo R, Varnum B, Brancolini C, Schneider C. Gas6 anti-apoptotic signaling requires NF-kappa B activation. *J Biol Chem* 2001; 276:31738-44; PMID:11425860; <http://dx.doi.org/10.1074/jbc.M104457200>
- [40] Stutz A, Golenbock DT, Latz E. Inflammasomes: too big to miss. *J Clin Invest* 2009; 119:3502-11; PMID:19955661; <http://dx.doi.org/10.1172/JCI40599>
- [41] Schroder K, Tschopp J. The inflammasomes. *Cell* 2010; 140:821-32; PMID:20303873; <http://dx.doi.org/10.1016/j.cell.2010.01.040>
- [42] Bensaad K, Cheung EC, Vousden KH. Modulation of intracellular ROS levels by TIGAR controls autophagy. *EMBO J* 2009; 28:3015-26; PMID:19713938; <http://dx.doi.org/10.1038/emboj.2009.242>
- [43] Wree A, Eguchi A, McGeough MD, Pena CA, Johnson CD, Canbay A, Hoffman HM, Feldstein AE. NLRP3 inflammasome activation results in hepatocyte pyroptosis, liver inflammation, and fibrosis in mice. *Hepatology* 2014; 59:898-910; PMID:23813842; <http://dx.doi.org/10.1002/hep.26592>
- [44] Fourcot A, Couchie D, Chobert MN, Zafrani ES, Mavier P, Laperche Y, Brouillet A. Gas6 deficiency prevents liver inflammation, steatohepatitis, and fibrosis in mice. *Am J Physiol Gastrointest Liver Physiol* 2011; 300:G1043-53; PMID:21350191; <http://dx.doi.org/10.1152/ajpgi.00311.2010>
- [45] Bárcena C, Stefanovic M, Tutusaus A, Joannas L, Menéndez A, García-Ruiz C, Sancho-Bru P, Mari M, Caballeria J, Rothlin CV, et al. Gas6/Axl pathway is activated in chronic liver disease and its targeting reduces fibrosis via hepatic stellate cell inactivation. *J Hepatol* 2015; 63:670-8.
- [46] Park HJ, Lee SJ, Kim SH, Han J, Bae J, Kim SJ, Park CG, Chun T. IL-10 inhibits the starvation induced autophagy in macrophages via class I phosphatidylinositol 3-kinase (PI3K) pathway. *Mol Immunol* 2011; 48:720-7; PMID:21095008; <http://dx.doi.org/10.1016/j.molimm.2010.10.020>
- [47] Pineda-Torra I, Gage M, de Juan A, Pello OM. Isolation, culture, and polarization of murine bone marrow-derived and peritoneal macrophages. *Methods Mol Biol* 2015; 1339:101-9; PMID:26445783; [http://dx.doi.org/10.1007/978-1-4939-2929-0\\_6](http://dx.doi.org/10.1007/978-1-4939-2929-0_6)
- [48] Sander LE, Sackett SD, Dierssen U, Beraza N, Linke RP, Müller M, Blander JM, Tacke F, Trautwein C. Hepatic acute-phase proteins control innate immune responses during infection by promoting myeloid-derived suppressor cell function. *J Exp Med* 2010; 207:1453-64; PMID:20530204; <http://dx.doi.org/10.1084/jem.20091474>
- [49] Lodder J, Denaës T, Chobert MN, Wan J, El-Benna J, Pawlotsky JM, Lotersztajn S, Teixeira-Clerc F. Macrophage autophagy protects against liver fibrosis in mice. *Autophagy* 2015; 11:1280-92; PMID:26061908; <http://dx.doi.org/10.1080/15548627.2015.1058473>
- [50] Lu Y, Leung TM, Ward SC, Nieto N. Partial deletion of argininosuccinate synthase protects from pyrazole plus LPS-induced liver injury by decreasing nitrosative stress. *Am J Physiol Gastrointest Liver Physiol* 2012; 302:G287-95; PMID:22052013; <http://dx.doi.org/10.1152/ajpgi.00375.2011>
- [51] Xu H, Garver H, Fernandes R, Galligan JJ, Fink GD. Altered L-type Ca<sup>2+</sup> channel activity contributes to exacerbated hypoperfusion and mortality in smooth muscle cell BK channel-deficient septic mice. *Am J Physiol Regul Integr Comp Physiol* 2014; 307:R138-48; PMID:24829499; <http://dx.doi.org/10.1152/ajpregu.00117.2014>
- [52] Mao K, Chen S, Chen M, Ma Y, Wang Y, Huang B, He Z, Zeng Y, Hu Y, Sun S, et al. Nitric oxide suppresses NLRP3 inflammasome activation and protects against LPS-induced septic shock. *Cell Res* 2013; 23:201-12; PMID:23318584; <http://dx.doi.org/10.1038/cr.2013.6>